2004 WHOI/NOAA Stratus2004
Field Program on the NOAA Ship Ronald H. Brown
December 5 – December 23, 2004
Results from the ETL Cloud and Flux Group, Texas A&M University, and University of Miami Measurements

C. W. Fairall, E. F. Bradley, J. Hare, D. Wolfe, Efthymios Serpetzoglou, Jason Tomlinson
NOAA Environmental Technology Laboratory
Boulder, CO USA
December 22, 2004

1. Background on Measurement Systems

The ETL air-sea flux and cloud group conducted measurements of fluxes and near-surface bulk meteorology during the fall field program to recover the WHOI Ocean Reference Station buoy at 20 S Latitude 85 W Longitude. The ETL flux system was installed initially in New England in June 2004, used on ICARTT field study in July and August, and brought back into full operation in Puerto Rico in late September, 2004. The system was operated on the TAO tender cruise prior to the Stratus cruise. The air-sea flux system consists of six components. (1) A fast turbulence system with ship motion corrections mounted on the jackstaff. The jackstaff sensors are: INUSA Sonic anemometer, OPHIR IR-2000 IR-hygrometer, LiCor LI-7500 fast CO2/hygrometer, and a Systron-Donner motion-pak. (2) A mean T/RH sensor in an aspirator on the jackstaff. (3) Solar and IR radiometers (Eppley pyranometers and pyrgeometer) mounted on top of a seatainer on the 02 deck. (4) A near surface sea surface temperature sensor consisting of a floating thermistor deployed off port side with outrigger. (5) An optical rain gauge mounted on the bow tower. Slow mean data (T/RH, PIR/PSP, etc) are digitized on Campbell 21x datalogger and transmitted via RS-232 as 1-minute averages. A central data acquisition computer logs all sources of data via RS-232 digital transmission:

1. Sonic Anemometer
2. Licor CO2/H2O
3. Slow means (Campbell 21x)
4. Not used
5. OPHIR hygrometer
6. Systron-Donner Motion-Pak
7. Ship's SCS
8. ETL GPS

The 8 data sources are archived at full time resolution. At sea we run a set of programs each day for preliminary data analysis and quality control. As part of this process, we produce a quick-look ascii file that is a summary of fluxes and means. The data in this file come from three sources: The ETL sonic anemometer (acquired at 21.3 Hz), the ships SCS system (acquired at 2 sec intervals), and the ETL mean measurement systems (sampled at 1 sec and averaged to 1 min). The sonic is 5 channels of data; the SCS file is 15 channels, and the ETL mean system is 42 channels. A series of programs are run that read these data files, decode them, and write daily text files at 1 min time resolution. A second set of programs reads the daily 1-min text files, time

matches the three data sources, averages them to 5 or 30 minutes, computes fluxes, and writes new daily flux files. The 5-min daily flux files have been combined and rewritten as a single file to form the file *flux_5hf_stratus_04.txt*. The 1-min daily ascii files are stored as *proc_nam_dayDDD.txt* (nam='pc', 'scs', or 'son'; DDD=yearday where 000 GMT January 1, 2004 =1.00). File structure is described in the original matlab files that write the data, *prt_nam_03.m*.

ETL/Flux and UM also operated six remote systems: a Vaisala CT-25K cloud base ceilometer, a 94 GHz vertically pointed FM-CW Doppler cloud radar, a 20.6-31.65-90.0 GHz microwave radiometer, a 35GHz Doppler cloud radar, a 915 MHz Doppler wind profiler, and the RHB's scanning Doppler C-band radar.. The ceilometer is a vertically pointing lidar that determines the height of cloud bottoms from time-of-flight of the backscatter return from the cloud. The time resolution is 30 seconds and the vertical resolution is 15 m. The raw backscatter profile and cloud base height information deduced from the instrument's internal algorithm are stored in daily files with the naming convention *CRVYYDDD.raw* where YY=04 and DDD=julian day. File structure is described in *ceilo_readme_stratus04.txt*.

ETL/Flux and UM used an integrated system in a seatainer that includes a Doppler K-band cloud radar (MMCR) and the 3-channel microwave radiometer. The UM FM-CW 94-GHz radar was mounted on a tripod on the deck and the data system was in the seatainer. The cloud radar systems can be used to deduce profiles of cloud droplet size, number concentration, liquid water concentration etc. in stratus clouds. If drizzle (i.e., droplets of radius greater than about 50 μm) is present in significant amounts, then the microphysical properties of the drizzle can be obtained from the first three moments of the Doppler spectrum. The MMCR radar is extremely sensitive and can detect most cirrus and fair weather cumulus clouds. The Doppler capability can also be used to measure in-cloud vertical velocity statistics. The UM radar is less sensitive but is ideal to detect drizzle and heavier cloud amounts. The C-band radar was operated continuously with a scan sequence program consisting of alternating a 0.5 deg elevation survey scan, RHI's, and a multiple elevation angle volume scan.

A second seatainer on the 02 deck housed an aerosol measurement system from the Texas A&M University. The Aerosol Research Group of Texas A&M University continuously monitored the aerosol distribution and concentration using a Tandem Differential Mobility Analyzer (TDMA) throughout the Stratus 2004 cruise.

Particularly in the latter half of the cruise, cloud cover was quite variable and sometimes cloud patterns change remarkably rapidly. For the record, five or six times a day photographs have been taken of the sky in four directions relative to the ship (over starboard, astern, port, and bow), especially at times of rapid cloud development. The timing of each set of four photographs has been carefully noted so that the directions can be converted to earth coordinates, knowing the ship's heading at that time.

2. Selected Samples

a. Flux Data

Preliminary flux data is shown for yearday=345 (December 10, 2004) as the RHB approaches the buoy site at 20 S 85 W (Fig. 1.). The time series of ocean and air temperature is given in Fig. 2. The water temperature is about 19.5 C and the air temperature is about 19.3 C. The true wind direction (Fig. 3) and true wind speed (Fig. 4) show modulation by boundary-layer

scale organization. The effect of clouds on the downward solar flux is shown in Fig. 5 and on the IR flux in Fig. 6. For the solar flux, broken clouds are apparent in the jagged form of the curve during the afternoon. For IR flux, clear skies have values of about 330 Wm^{-2} and cloudy skies values around 400 Wm^{-2}. The IR flux suggests some small breaks in the clouds in late afternoon. Fig. 7 shows the time series of four of the five primary components of the surface heat balance of the ocean (solar flux is left out). The largest term is the latent heat (evaporation) flux, followed by the net IR flux (downward minus upward); the sensible heat flux and the flux carried by precipitation are very small. We are using the meteorological sign convention for the turbulent fluxes so all three fluxes actually cool the interface in this case. The time series of net heat flux to the ocean is shown in Fig. 8. The sum of the components in Fig. 7 is about -100 Wm^{-2}, which can be seen in the night time values; the large positive peak during the day is due to the solar flux.. The integral over the entire day gives an average flux of 72 Wm^{-2}, indicating strong warming of the ocean mixed layer even on an overcast day.

b. Remote Sensing Data

A sample ceilometer 24-hr time series for cloud base height for December 10 is shown in Fig. 9. This day had 98% cloud cover and two sets of cloud base heights: the dominant stratocumulus layer with cloud bases 900 to 1100 m and occasional lower level 'scud' clouds with bases about 500 m. Small amounts of drizzle can be seen as the few low-altitude dots early in the day. A sample time-height cross section (Fig. 10) from the UM cloud radar is shown for a 24-hr period on December 10. The panels indicated the intensity of the return (upper), the mean fall velocity of the scattering droplets (middle panel), and the Doppler width of the return. This happens to be a day with low cloud cover; clouds are fairly thin with tops at 1.0 - 1.2 km. Light drizzle events are apparent as the 0830 and 1430; the radar is much more sensitive to drizzle than the ceilometer. The ETL MMCR suffered a component failure the fourth day of the cruise, so no data will be shown.

A time series from the microwave radiometer is shown in Fig. 11. The middle panel shows the integrated liquid water path (LWP) of the stratus clouds. The peak early in the evening (0300) corresponds to light drizzle observed on the ceilometer (lower dots in Fig. 9). Note that LWP declines steadily after sunrise (345.45 GMT) except for the blip associated with the scud cloud at 2000 GMT.

The scanning C-band (5 cm wavelength) Doppler radar ran continuously recording large volumes of data (no examples shown here). A sample time-height cross section from the wind profiler raw moment data for the vertical beam is shown (Fig. 13) for December 10. The wind profiler operates at 33 cm wavelength where it is sensitive enough to detect returns from turbulent variations in radar refractive index, principally associated with gradients in atmospheric moisture; it is also sensitive to precipitation. Sensitivity to moisture gradients causes the marine inversion to show up clearly as the band at 1.3 km. Both of these factors cause improved height performance in stormy conditions. The winds are shown in Fig. 13 as a standard meteorological wind bard plot (time going right to left). Winds in the boundary layer are predominately from the SE.

3. Cruise Summary Results

a. Basic Time Series

The ship track for the entire cruise is shown in Fig. 14. The 5-min resolution time series for sea and air temperature are shown in Fig. 15 and for wind speed and N/E components in Fig.16. The change in conditions for the first day of the record is associated with the run southwest from Arica, Chile, to the DART buoy at 20 S. The near-surface sea-air temperature is near zero in the vicinity of the WHOI buoy; this is consistent with the buoy climatology for December. The mean diurnal cycle for the wind components (Fig. 17) shows a weak diurnal variation with a minimum at 13-15 local time. There is also a weak semidiurnal cycle (atmospheric tide?) in the wind and air temperature variables. Primarily because of the healthy wind speeds (about 8 m/s), there is only a small diurnal signal (0.15 C) in the sea surface temperature. Time series for flux quantities are shown as daily averages. Fig. 18 gives the flux components and Fig. 19 the cloud forcing for net surface radiative fluxes. Cloud forcing is the difference between the measured radiative flux and that which would be expected if there were no clouds. It is essentially a measure of the effect of clouds on the energy budget of the ocean. A negative cloud forcing implies the cloud cools the ocean (e.g., by reflecting solar flux).

The diurnal cycle of cloudiness (i.e., thinning or clearing after local noon) at 20 S leads to fairly large values of net heat flux and solar flux at 20 S; afternoon clearing leads to much greater 24-hr average solar flux. Just for amusement, bulk meteorological variables and turbulent heat fluxes are shown for the transect from 70 W to 90 W along 20 S in Fig. 20. This shows the winds increasing gradually away from the coast and a minimum in latent heat flux at 80 W. The return transect was taken at an angle towards Valparaiso, Chile (see Fig. 14). The W to E transect (Fig. 21) looks similar initially, but in the second half colder water is encountered nearing the coast versus warmer water near the coast in Fig. 20. The coastal jet is apparent as the 12.5 m/s peak in the wind speed at about 74 W.

The number distribution and concentration of aerosols from 0.010-μm to 0.800-μm is shown in Fig. 22 . The distribution is strongly bimodal throughout the cruise as a result of cloud processing, which is typical of the marine boundary layer. The concentration varies with a time scale of several days. This is the result of the complex interaction between entrainment, advection, production and scavenging of aerosols. The average total number concentration from December 8th to the 18th was 350 ± 150 (cm^{-3}), with an average CCN (diameter greater than about 0.1-μm) concentration of 182 ± 44 (cm^{-3}) and an average non-CCN concentration of 168 ± 82 (cm^{-3}).

b. Boundary Layer and Cloud Properties

Beginning on December 6 and ending on December 22 we completed 75 successful rawinsonde launches. While at the WHOI buoy sondes were done 6 times daily; otherwise, they were done 4 times daily. A time-height color contour plot of potential temperature is shown in the upper panel of Fig. 23; the lower panel shows the relative humidity. A pronounced temperature inversion is evident at approximately 1.7-2.5 km. This inversion defines the BL depth which is initially about 1.7 km but on day 347 (Dec. 12) begins to increase and reaches 2.5 km by day 353 (Dec. 18). The large scale moisture feature evident in the RH plot at 23 km in the beginning of the record descends steadily to 5 km by Dec. 18. This descent rate is consistent

with a divergence of about 1.0E-6 s^{-1} . The time series of wind speed and direction are shown in Fig. 24. The winds are consistent with climatology, with southeasterlies prevailing within the boundary layer and westerlies aloft. The nominal height for the transition from westerlies to easterlies descended steadily during the experiment in coincidence with the moisture transition described above.

The time series of cloud base height from the ceilometer is shown in Fig. 25. Throughout the cruise the ceilometer was giving a fault code indicating optical feedback in the detection loop. This indicates a deterioration of the optical fiber that carries the signal to the detector. Thus, the ceilometer was operating at reduced sensitivity, especially during daytime when sunlight contaminates the detection of clouds. As a result, the ceilometer did not detect many clouds particularly the higher cloud bases later in the cruise; when clouds are detected, the cloud base height is accurate. The increase in cloud base height after 344 is consistent with the increase with inversion height. The time series of data from the microwave radiometer is shown in Fig. 26. The microwave radiometers are calibrated using a tipcal process that requires clear skies. This was done repeatedly in port, but after day 340 sky conditions did not permit new tipcals. Judging from the near-zero liquid water contents during limited periods with skies clear directly overhead, it appears that the calibration may have drifted to a positive bias later in the cruise. This will be evaluated in the future.

4. Intercomparisons

Intercomparisons are a key strategy in data quality assurance for the climate reference buoys and the use of research vessel measurements for climate-quality data archives. The ETL flux system is intended to produce measurements of turbulent flux bulk variables and radiative fluxes that have the required accuracy for climate research. For this cruise, a set of Intercomparisons were done for bulk meteorology and radiative fluxes.

*The ETL flux system acquired all relevant ship IMET-based measurements.
*ETL and ship radiative fluxes were compared with the WHOI buoy (sitting on the deck) and an array of IMET radiative sensors (mounted in an array on the 03 deck).
*A carefully executed set of psychrometer measurements were taken regularly during the cruise as a reference for air temperature and humidity.
*Direct measurements of turbulent fluxes from the ETL system were compared with bulk fluxes for the cruise.

a. ETL-Ship Comparisons

We compared ETL and ship measurements for wind speed and direction, water and air temperature, relative humidity, and solar and IR downward radiative flux. All measurements agreed within the accuracy required for flux evaluations. The ship wind system does experience flow blockage by the jackstaff for relative winds from the starboard side. One ship solar flux sensor read 4% higher than ETL. A second sensor was deployed for one day and it agreed with the ETL values within 1%. A detailed analysis will be done later.

b. Psychrometer Comparisons

As in some previous cruises, the accuracy of our Vaisala temperature and humidity measurements were checked against a hand-held Assman psychrometer. About 5 times throughout the day, when the wind was within ±90º of dead ahead, the Assman wet and dry bulb temperatures were sampled through either port or starboard chocks on the foredeck. These locations were adopted on earlier cruises, rather than over the bow itself, because they offer shading of the thermometers from the sun. The chocks are at a height of approximately 9 metres above the sea surface, compared with 15m for the Vaisala. These are spot values to be compared with our standard 5-minute averages, so some scatter is expected, but averaged over the cruise the comparison should be valid.

The CSIRO Assman is normally used for these measurements because its thermometers have been calibrated, but its ventilation motor broke its spring early in the cruise. An ETL Assman on board has therefore been used for the remainder of the cruise, after comparing the thermometers from the two instruments in a water bath. This indicated that a slight (-0.1ºC) correction was needed to both ETL thermometers. The comparison will be repeated more carefully at the end of the cruise, and the cruise-long data set re-calculated with all necessary corrections.

ETL, ship, and psychrometer values were compared for air temperature and specific humidity. The 9-meter psychrometer values were corrected to 15 m using similarity theory (based on the measured fluxes). The average correction was -0.01 C for temperature and -0.10 g/kg for humidity. The results for 79 samples are shown as scatter plots in Figs. 27 and 28; means are summarized in the table of mean values and standard deviations of differences given below:

	Mean ETL	Mean Ship	Mean Psy	Ensemble	$\sigma_{ETL\text{-}ship}$	$\sigma_{ETL\text{-}Pshch}$
T_{air} (C)	19.22	19.13	19.28	**19.21**	0.094	0.23
Q_{air} (g/kg)	10.07	10.00	9.97	**10.01**	0.090	0.23

The differences (0.09 C and 0.07 g/kg) in ETL and ship values are too small to be resolved by the psychrometer (accurate on average to 0.1 C and 0.1 g/kg). All three sensors are within required accuracy (0.1 C or g/kg) of the ensemble mean. To give a sense of the quality of the comparisons, the time series for specific humidity is shown with the ETL, ship, and Psychrometric values (Fig. 28).

c. Direct Versus Bulk Flux Algorithm Comparisons

ETL direct fluxes were computed using our standard software for motion corrections. This is a preliminary analysis; more detailed evaluation will be done in the future. Some 210 hourly values that passed screening criteria for the period 340-352 were used. The bulk algorithm (COARE model version 3.0) agreed well on average for sensible, latent, and momentum fluxes. Agreement was better than for many past cruises. Direct and bulk fluxes were compared by averaging in wind speed bins. Fig. 30 shows the results for the stratus04 cruise where means and medians are compared. Direct latent heat flux in this case is the average of OPHIR hygrometer covariance, OPHIR hygrometer inertial-dissipation, and Licor-7500 hygrometer covariance values. These same values are shown as an x-y scatter plot in Fig. 31.

Overall agreement for total mean/median latent heat flux is within 5%.

5. ETL Data Cruise Archive

Selected data products and some raw data were made available at the end of the cruise for the joint cruise archive. Some systems (radar, turbulence, microwave radiometer) generate too extravagantly to be practical to share. Compared to processed information, the raw data is of little use for most people. For the cloud radar and the C-band radar we have made available image files only; full digital data will be available later from the ETL website. For the microwave radiometer, the time series after some processing and averaging is given. No direct turbulent flux information is provided; that will be available after re-processing is done back in Boulder. However, bulk fluxes are available in the flux summary file

Data Archive Directories

Ceilo	Ceilometer files (processed file, images)
Flux	Air-sea flux files (processed flux files: daily files, cruise file, some m-files)
Sondes	Rawindsone files (.EDT)
Microwv	Microwave radiometer files (processed files; graphic display)
Radar	Image files from cloud radar
Reports	Documentation (cruise report, summary image files)
UProf	Image and data files from the wind profiler
Pics	Powerpoint files of sky pictures
UMFMCW	Image files from U. Miami 94-GHz FMCW cloud radar.
Satellite	Image files from the Terrascan satellite receiver

Contact:
C. Fairall
NOAA Environmental Technology Laboratory
325 Broadway
Boulder, CO USA 80305
303-497-3253
chris.fairall@noaa.gov

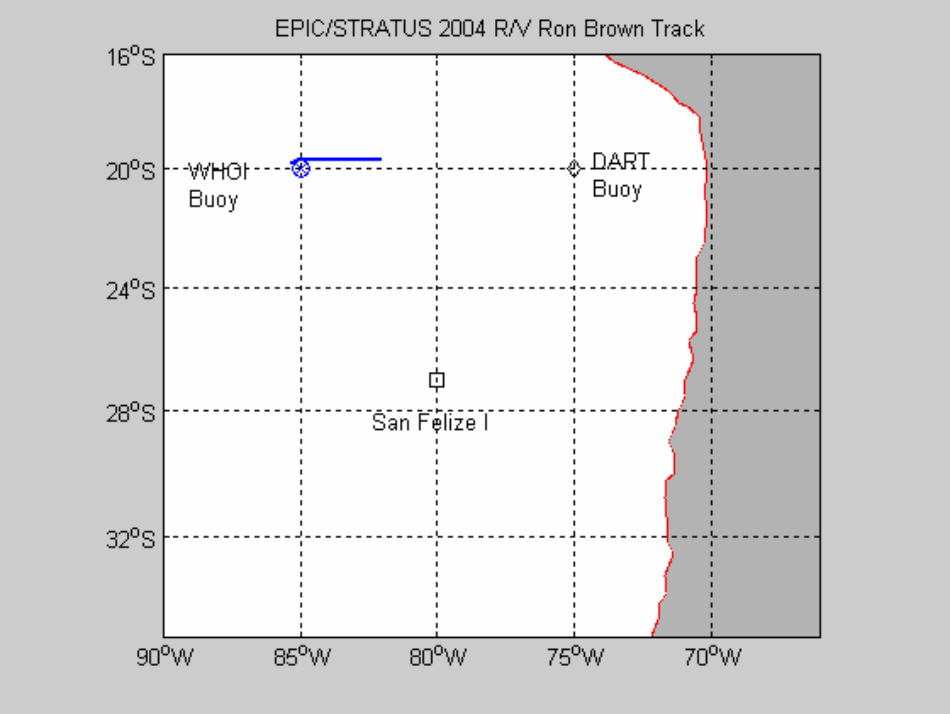

Figure 1. Cruise track for RBH on December10 (DOY 345).

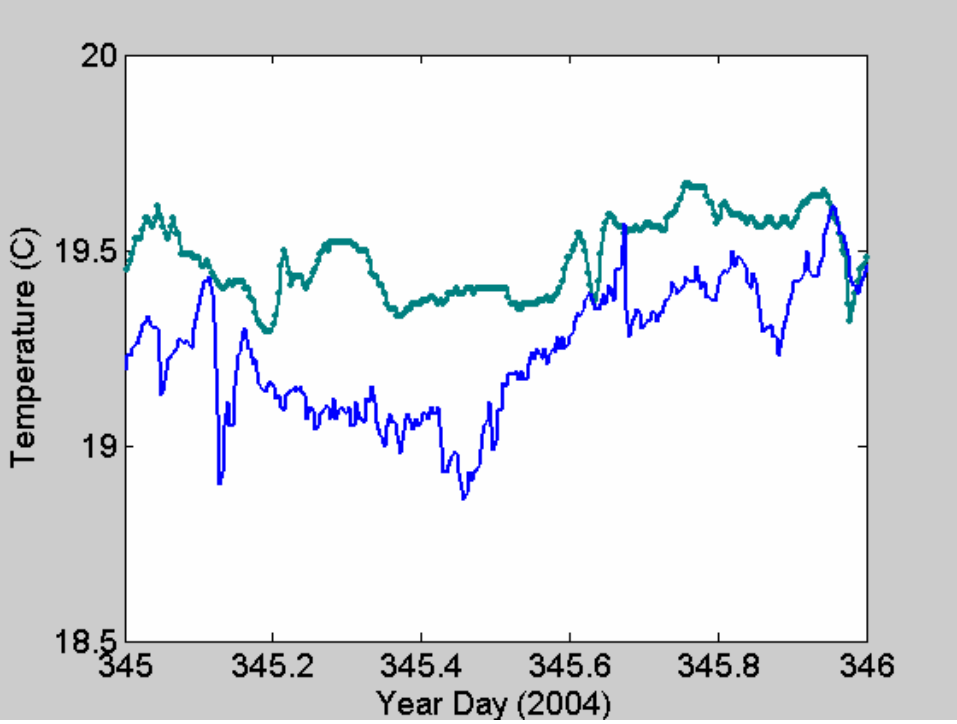

Figure 2. Time series of near-surface ocean temperature (green) and 15-m air temperature (blue).

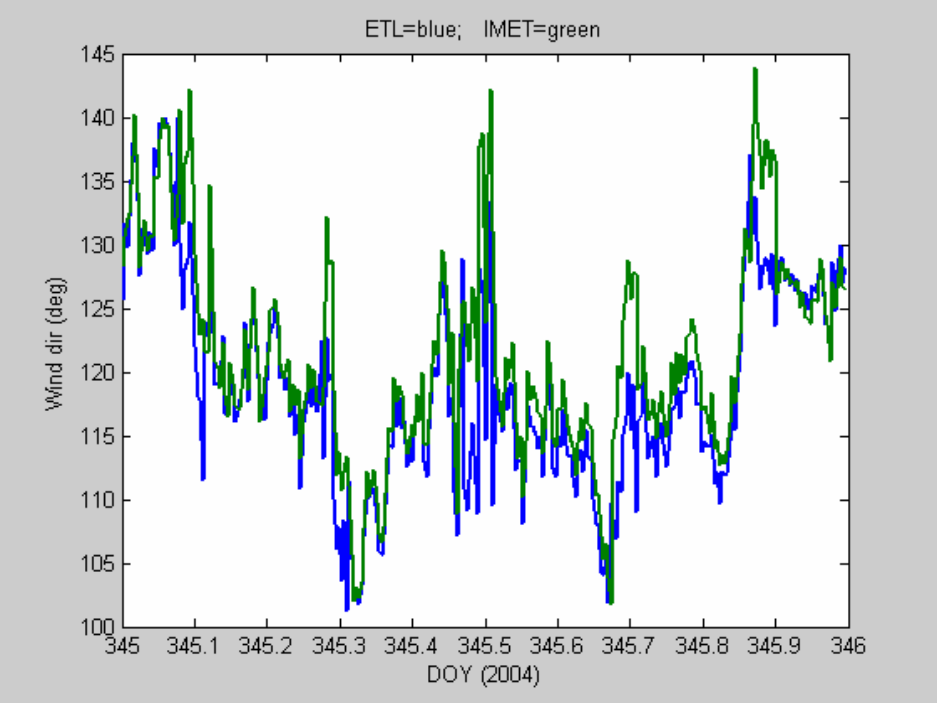

Figure 3. True wind direction from the ETL sonic anemometer (18 m) and the IMET propvane (15 m).

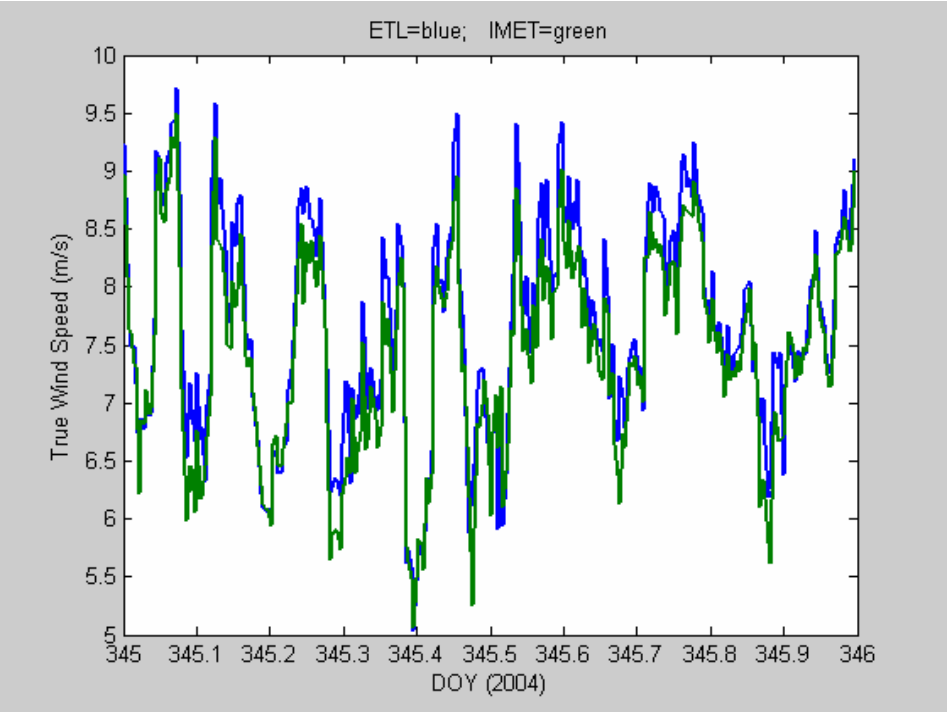

Figure 4. True wind speed from the ETL sonic anemometer (18 m) and the ship's propvane (15 m).

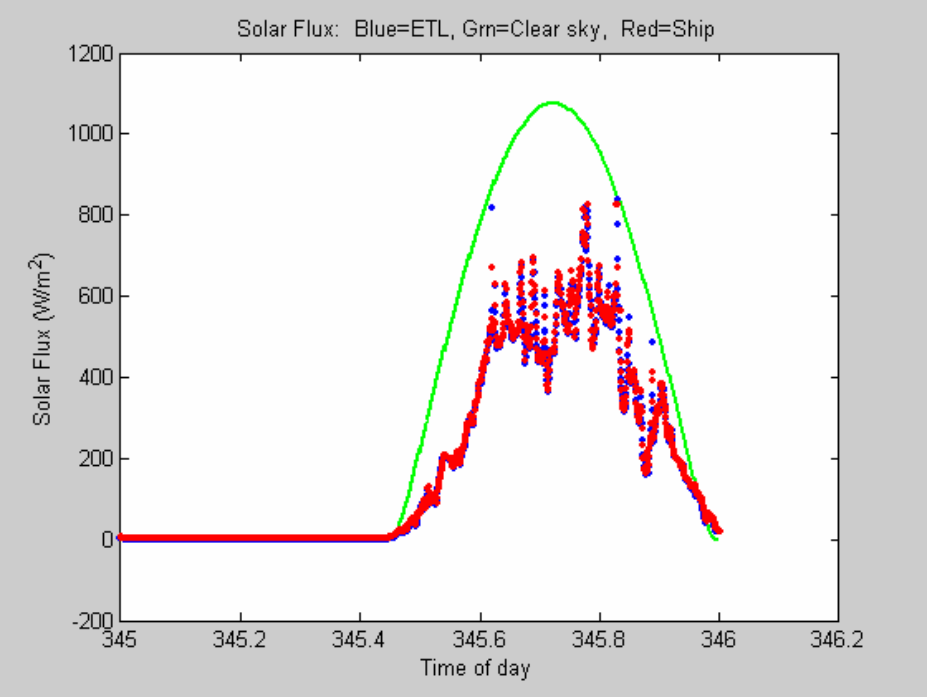

Figure 5. Time series of downward solar flux from ETL and ship Eppley sensors**.** The green line is a model of the expected clear sky value.

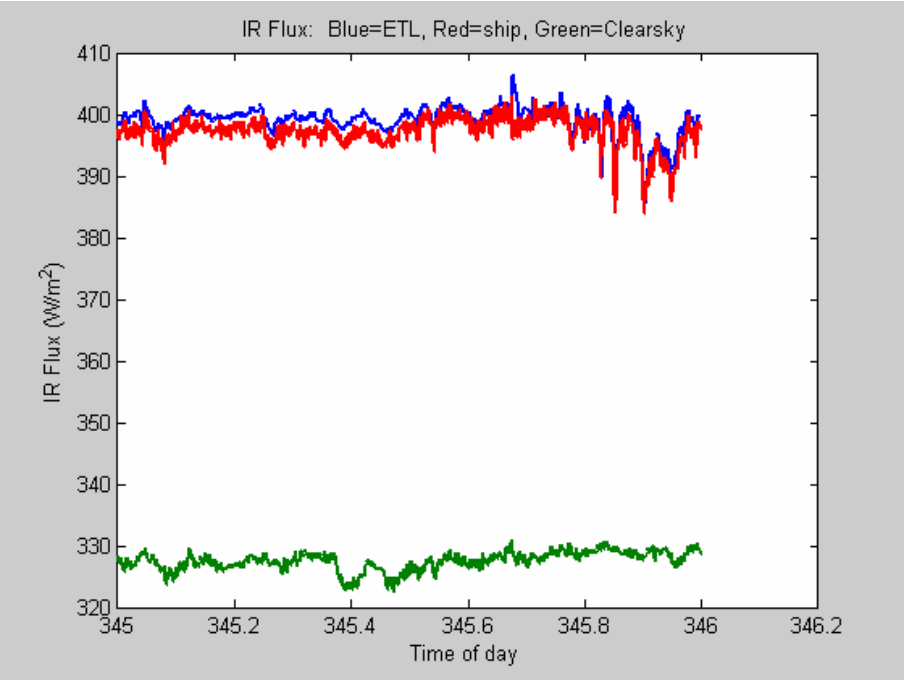

Figure 6. Time series of downward IR flux from ETL and ship Eppley sensors. The green line is a model of the expected clear sky value.

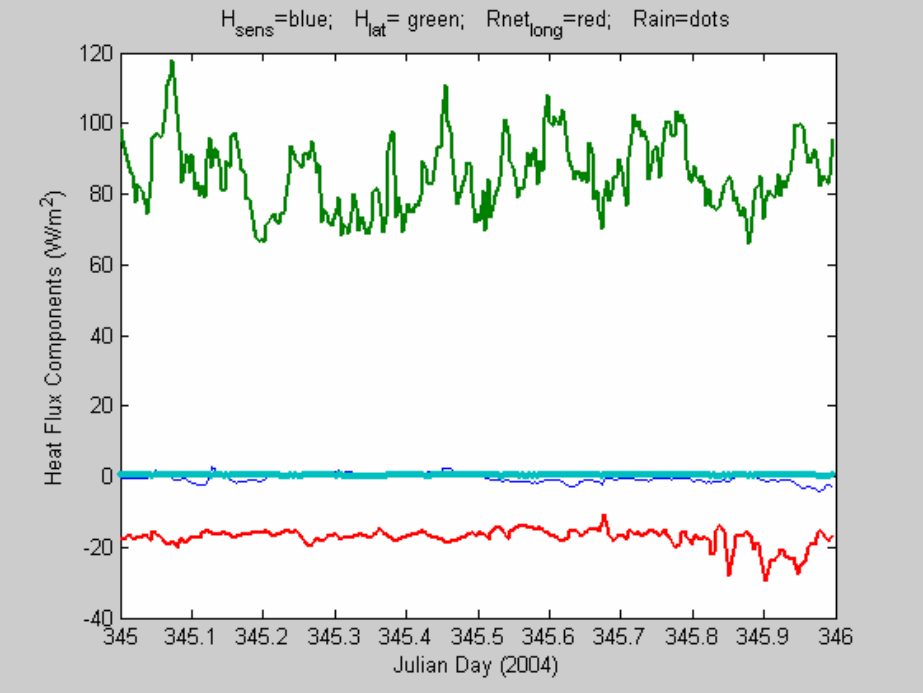

Figure 7. Time series of non-solar surface heat flux components: sensible (blue), latent (green), and net IR (red).

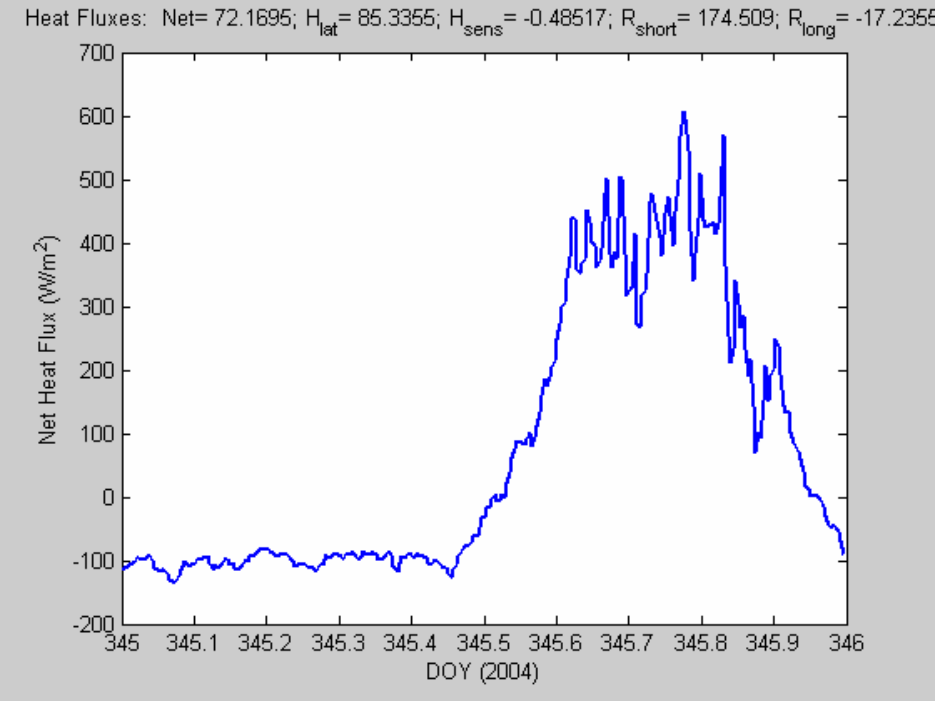

Figure 8. Time series of net heat flux to the ocean surface. The values at the top of the graph are the average for the day.

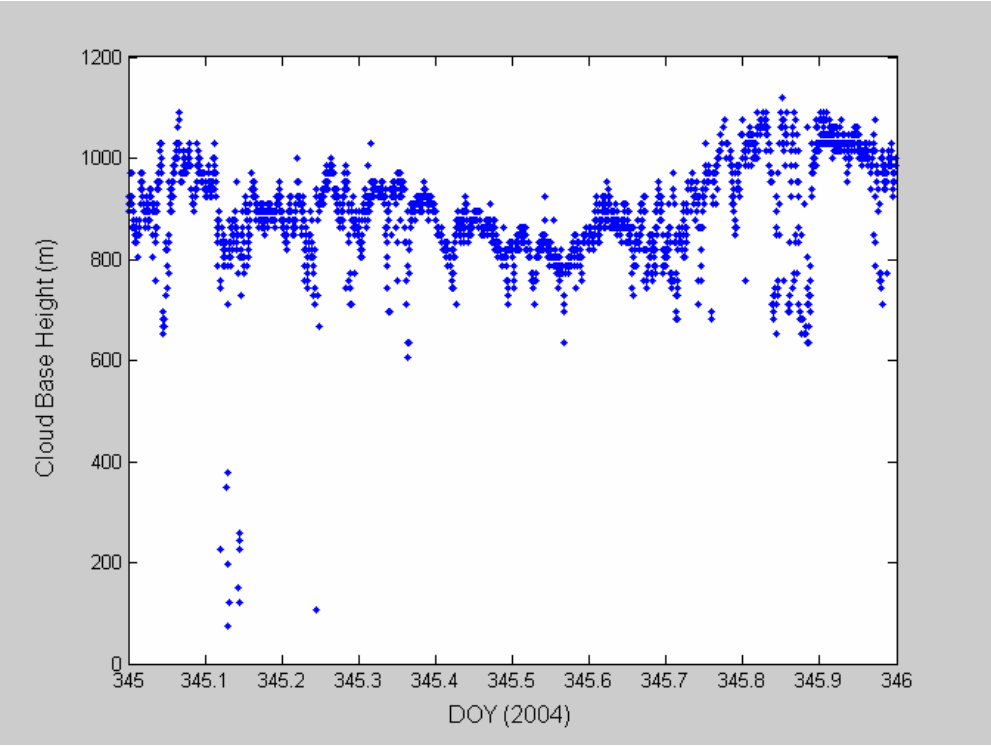

Figure 9. Cloud-base height information extracted from the ceilometer backscatter data.

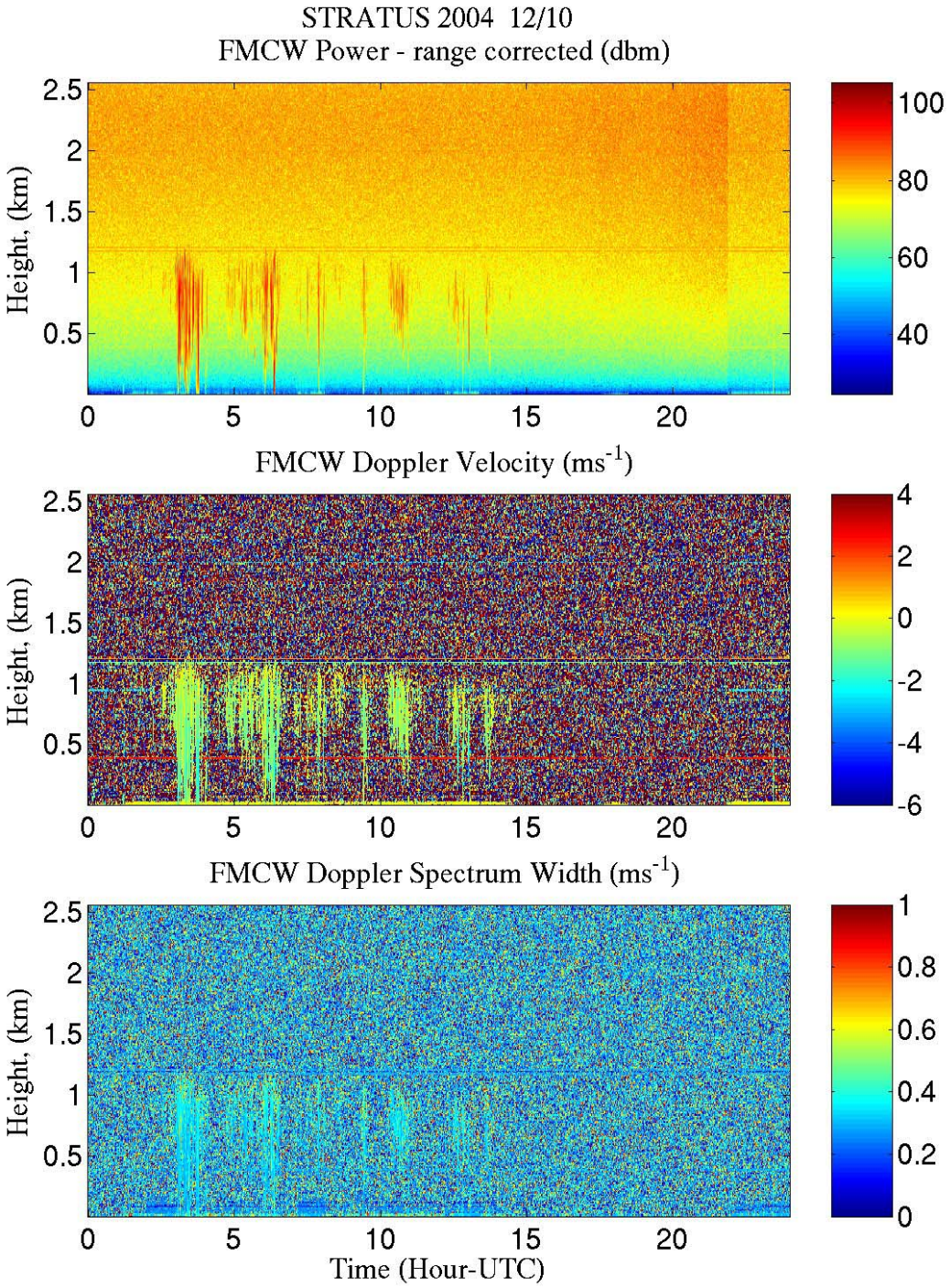

Figure 10. Time-height cross section data from 94 GHz cloud radar data for day 345 (December 10, 2004): upper panel, backscatter intensity; middle panel, mean Doppler vertical velocity; lower panel, Doppler width.. The deep vertical streaks are drizzle.

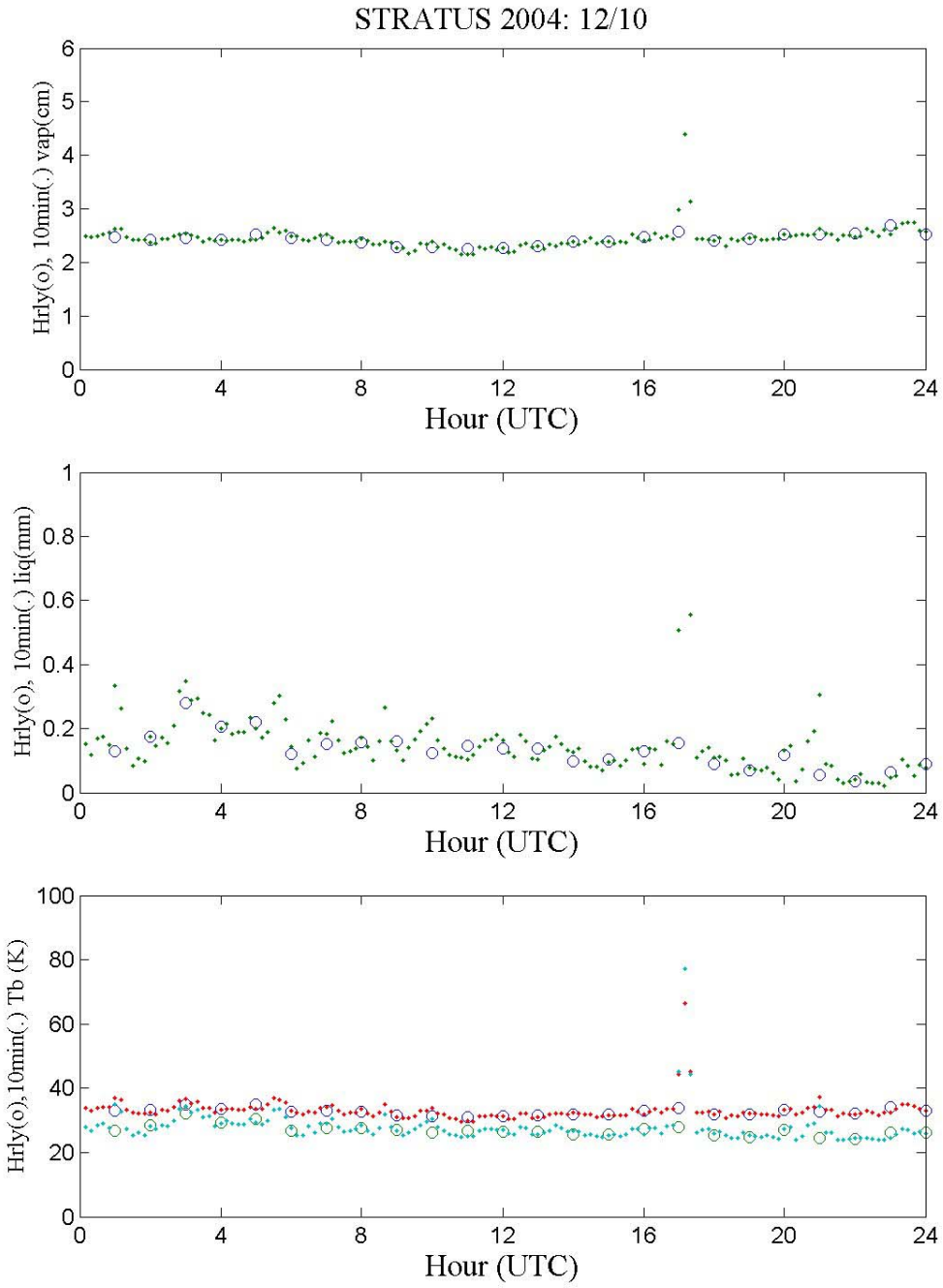

Figure 11. Time series of data from the 3-channel microwave radiometer: upper panel – column water vapor, middle panel – column water liquid, and bottom panel – brightness temperatures at 21 and 31 GHz.

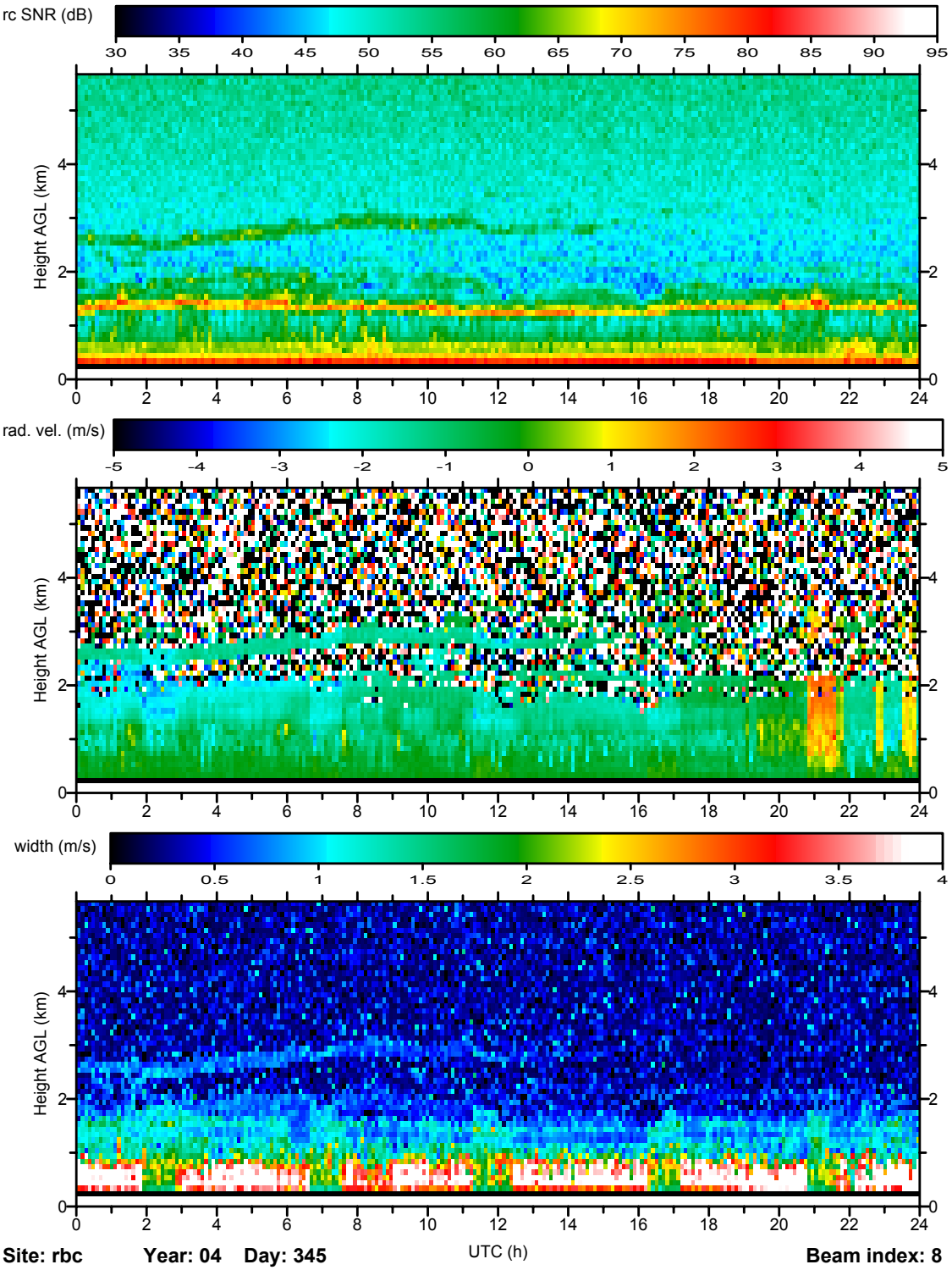

Figure 12. Time-height cross sections from RHB wind profiler for December 10: upper panel, backscatter intensity; middle panel, mean Doppler vertical velocity; lower panel, Doppler width. Bright yellow-red region at 1.3 km in upper panel is the boundary layer inversion. Red-white area on bottom of lower panel are sea clutter when the ship is underway; green areas in between are stops for CTD's.

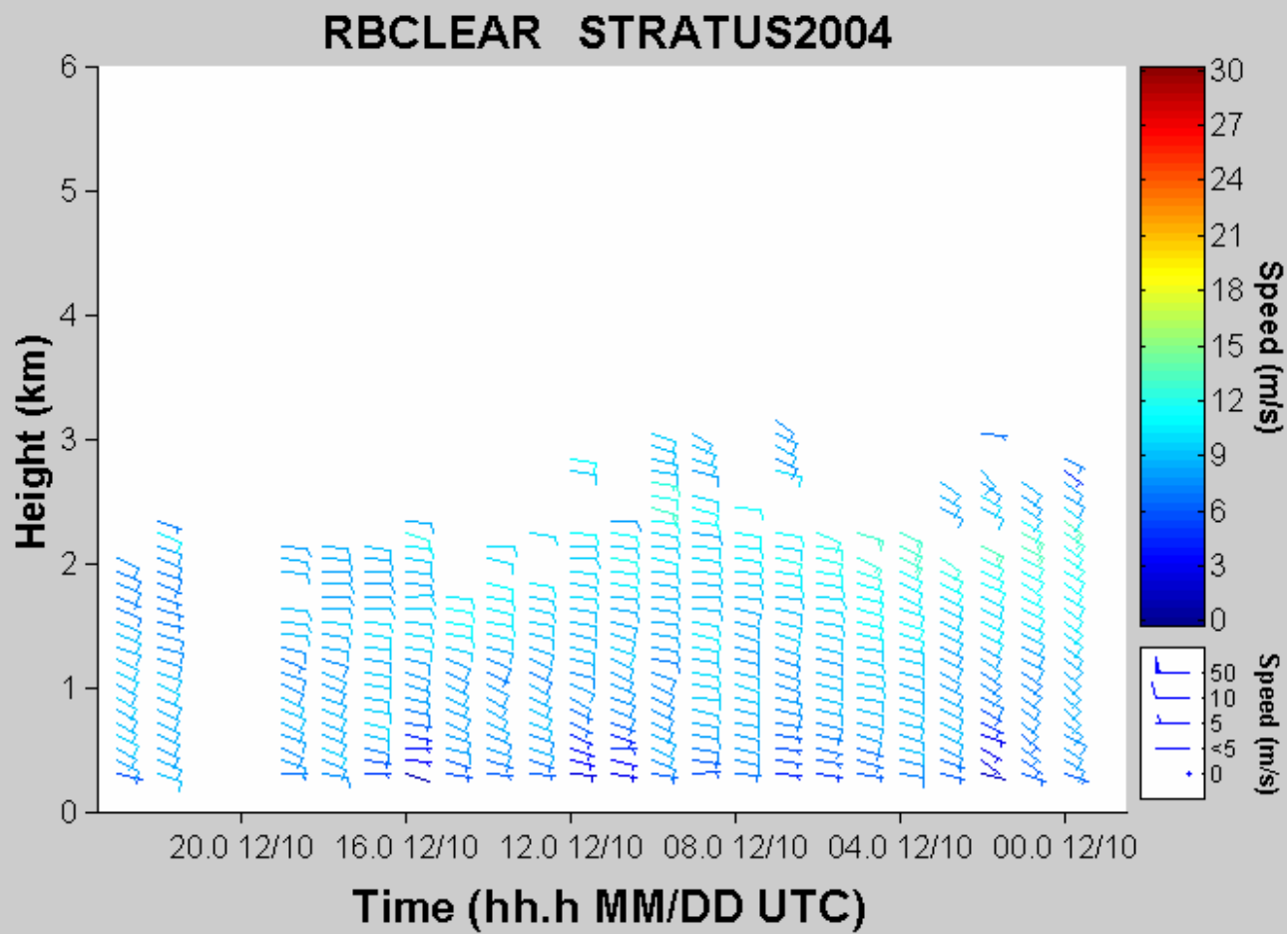

Figure 13. Time-height cross section of wind speed and direction for December 10. Barb orientation gives wind direction; color gives wind speed.

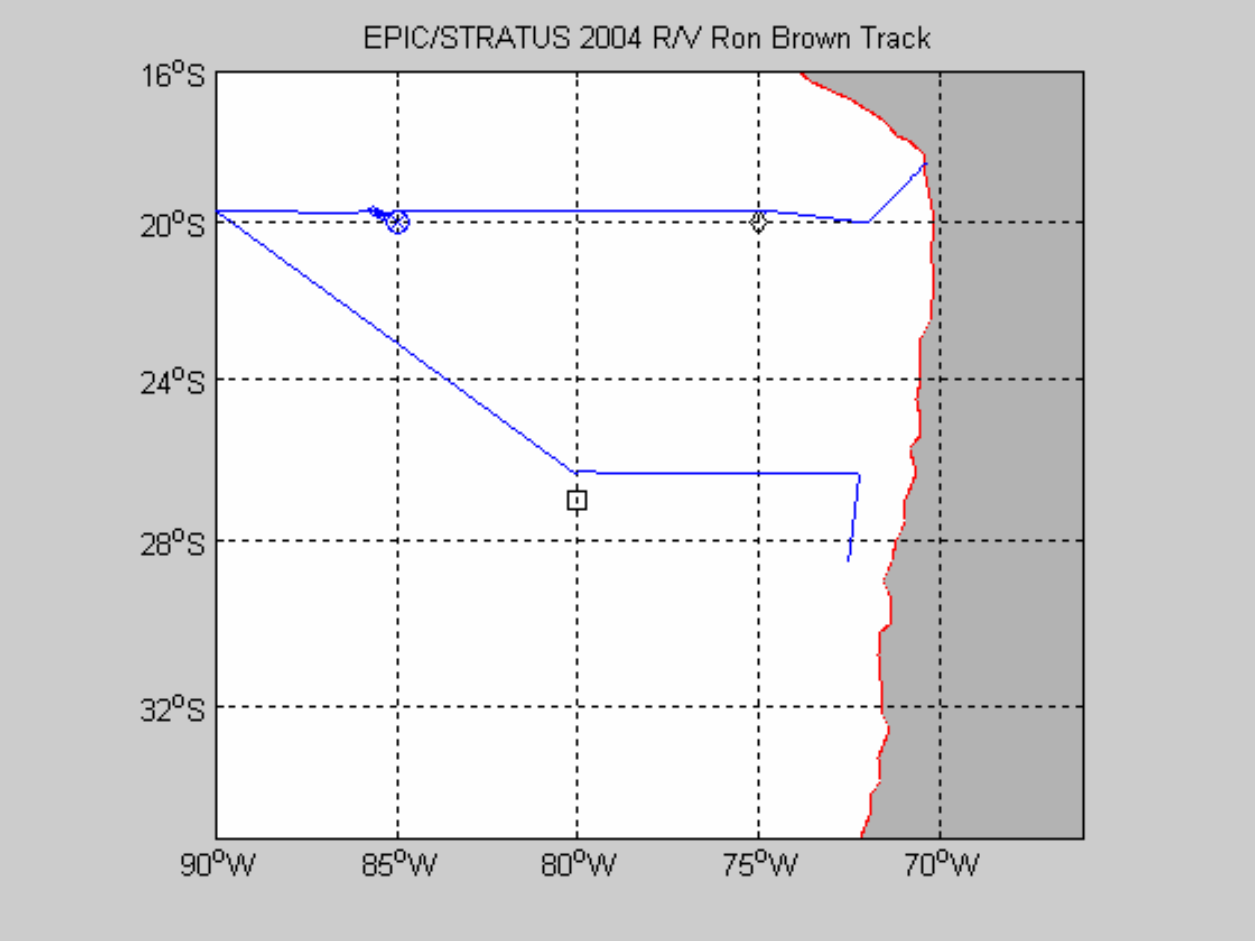

Figure 14. Cruise track for entire Stratus 2004 cruise.

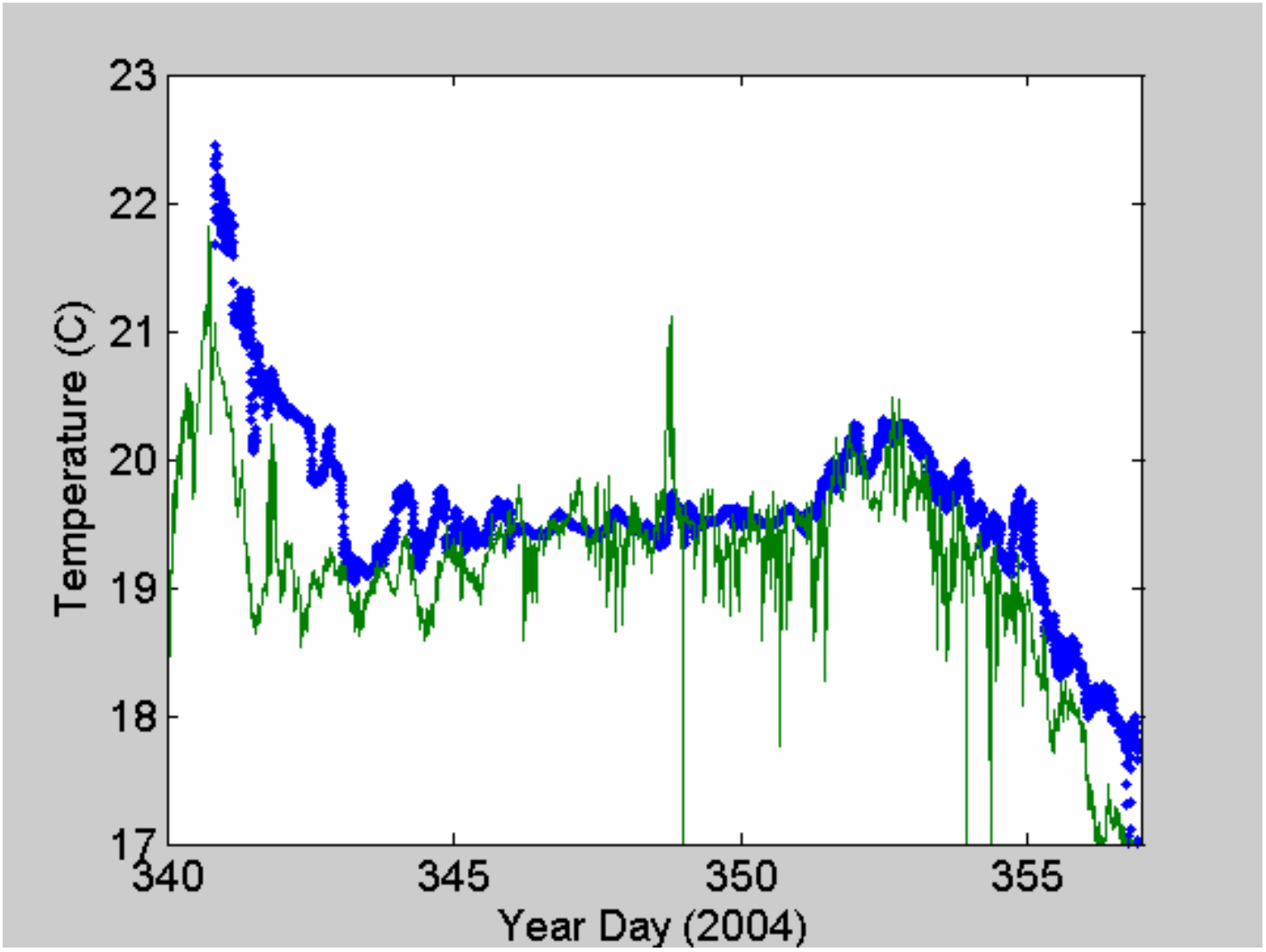

Figure 15 Time series of near-surface ocean temperature (blue) and 15-m air temperature (green) for the 2004 RHB Stratus cruise.

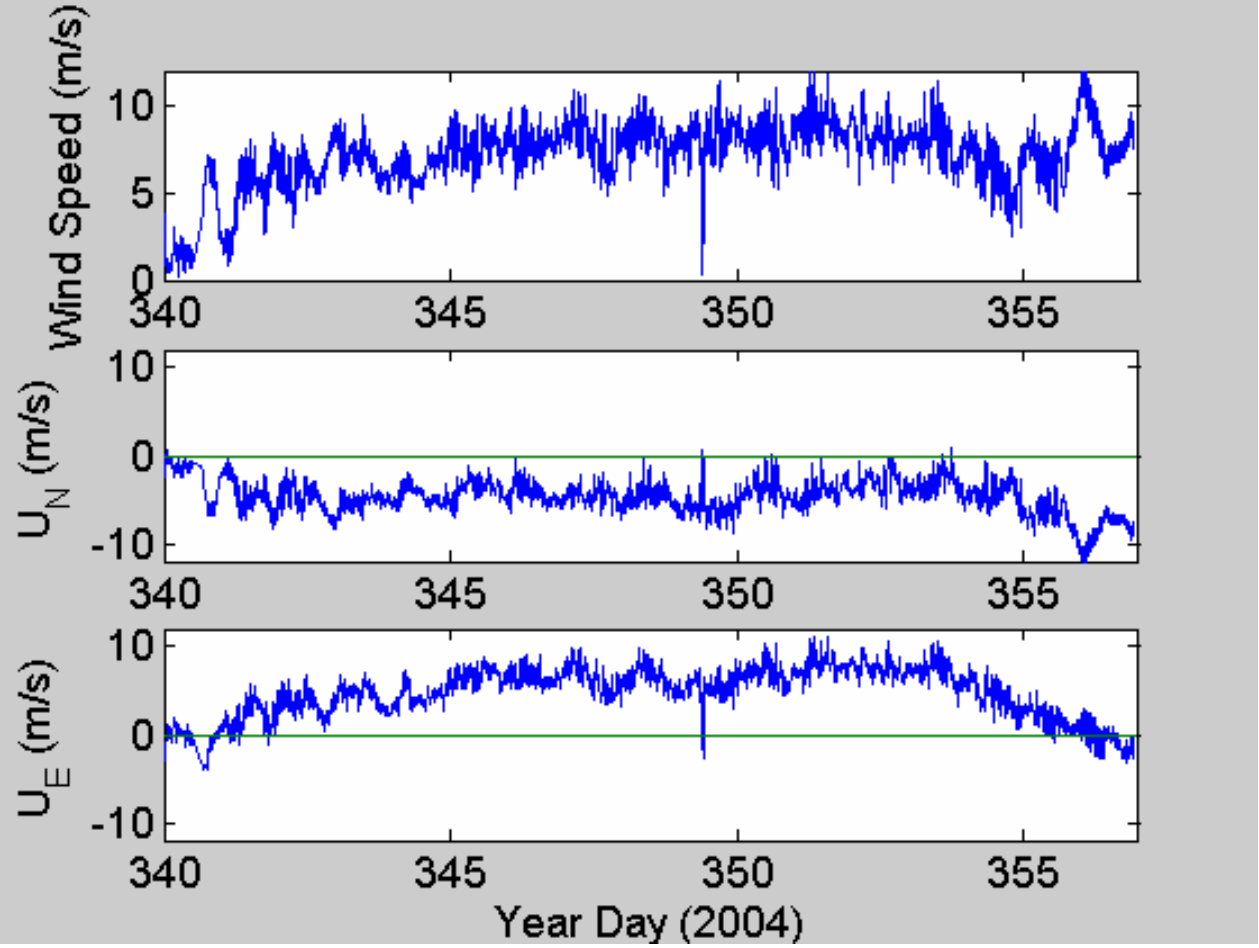

Figure 16. Time series of wind speed (upper panel), northerly component (middle panel), and easterly component (lower panel) for the 2004 RHB Stratus cruise.

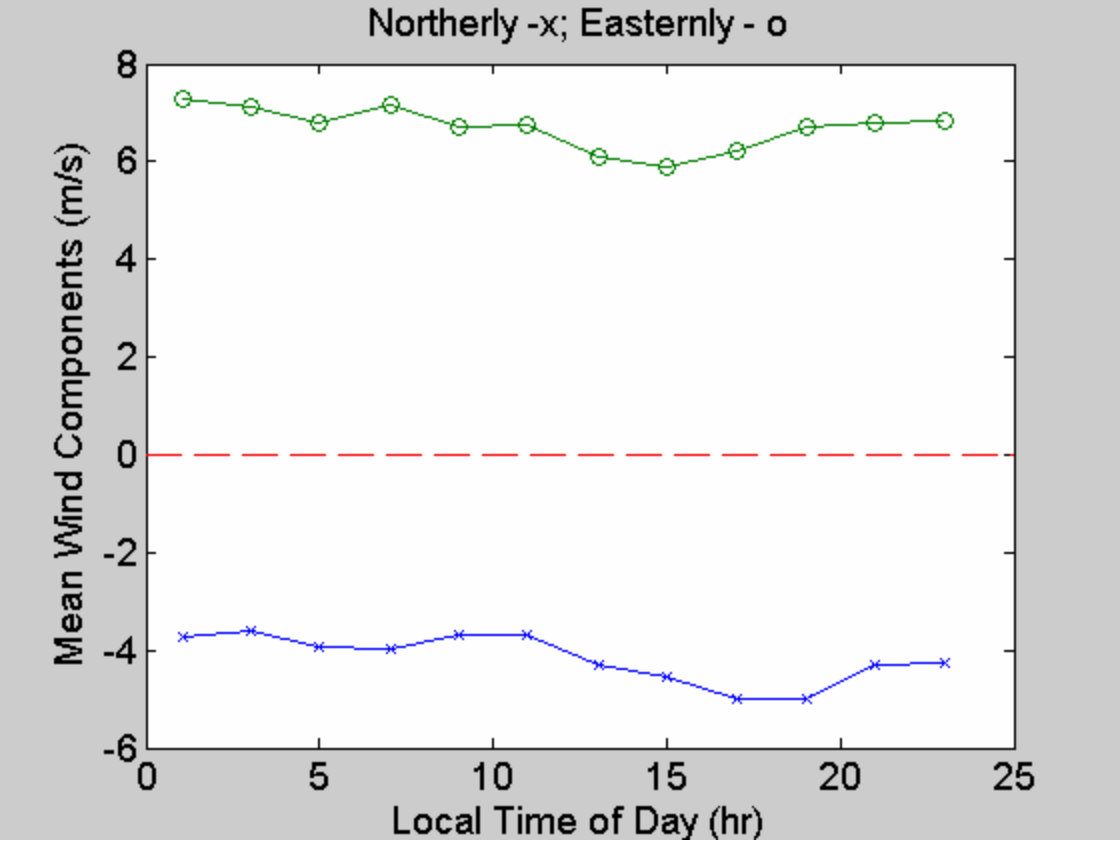

Figure 17. Diurnal average of northerly and easterly wind components for period near 20

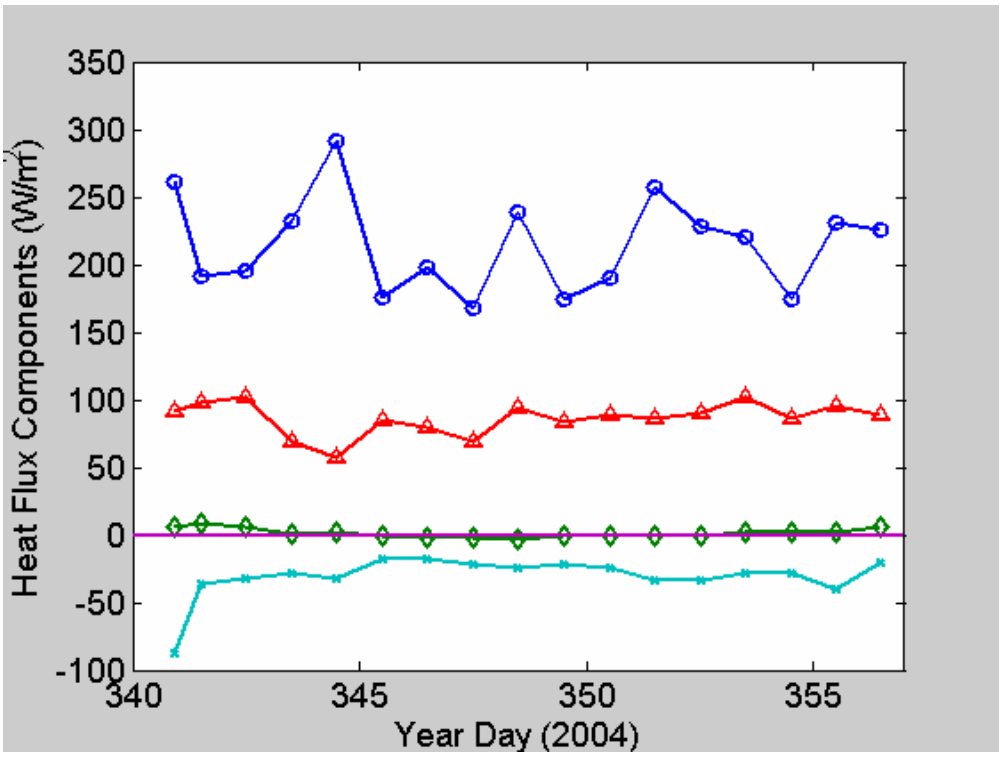

Figure 18. Time series of 24-hr average heat flux components: solar flux - circles; latent heat flux - triangles; sensible heat flux - diamonds; net IR flux x's.

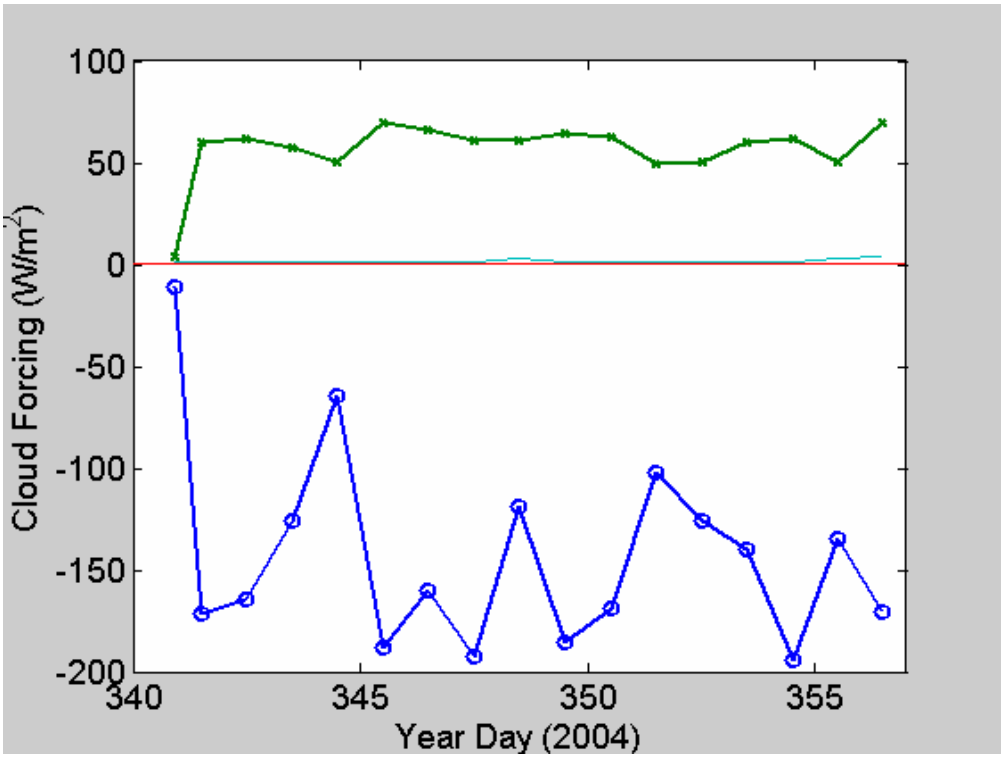

Figure 19. Time series of daily averaged radiative cloud forcing: IR CF (W/m^2) – green, Solar CF (W/m^2) – blue.

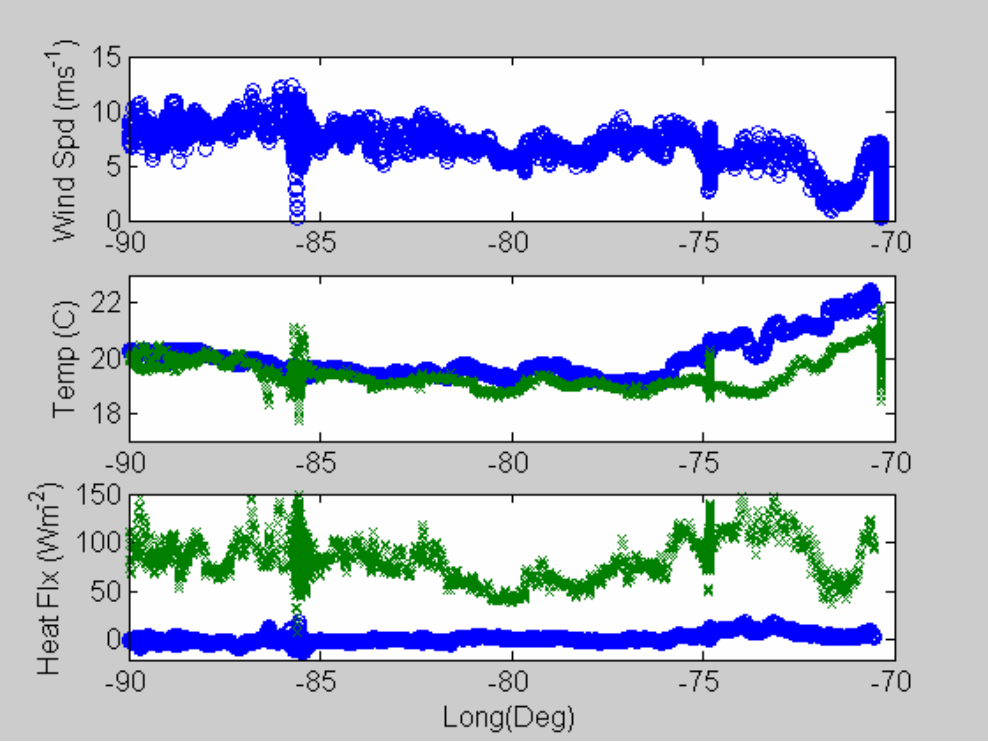

Figure 20. Selected variables from the E-W transect along 20 S. Upper panel is wind speed; the middle panel is sea surface temperature (blue) and air temperature (green); the lower panel shows sensible (blue) and latent (green) heat fluxes.

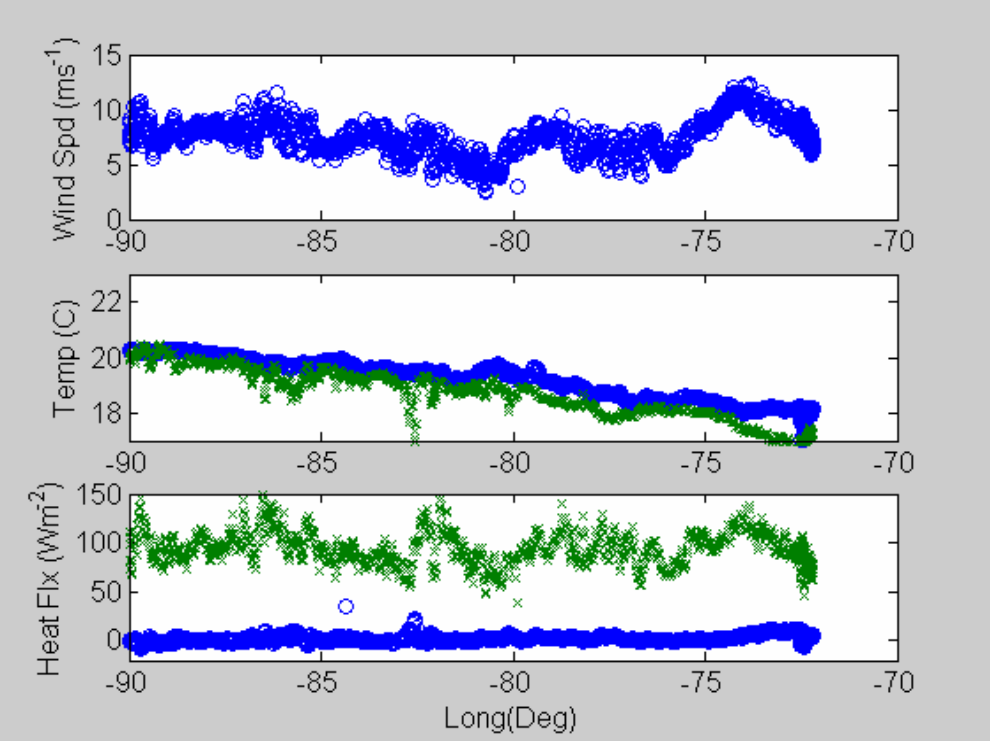

Figure 21. Same as Fig. 20, but for the W-E transect from 20 S 90W to 28 S 72 W.

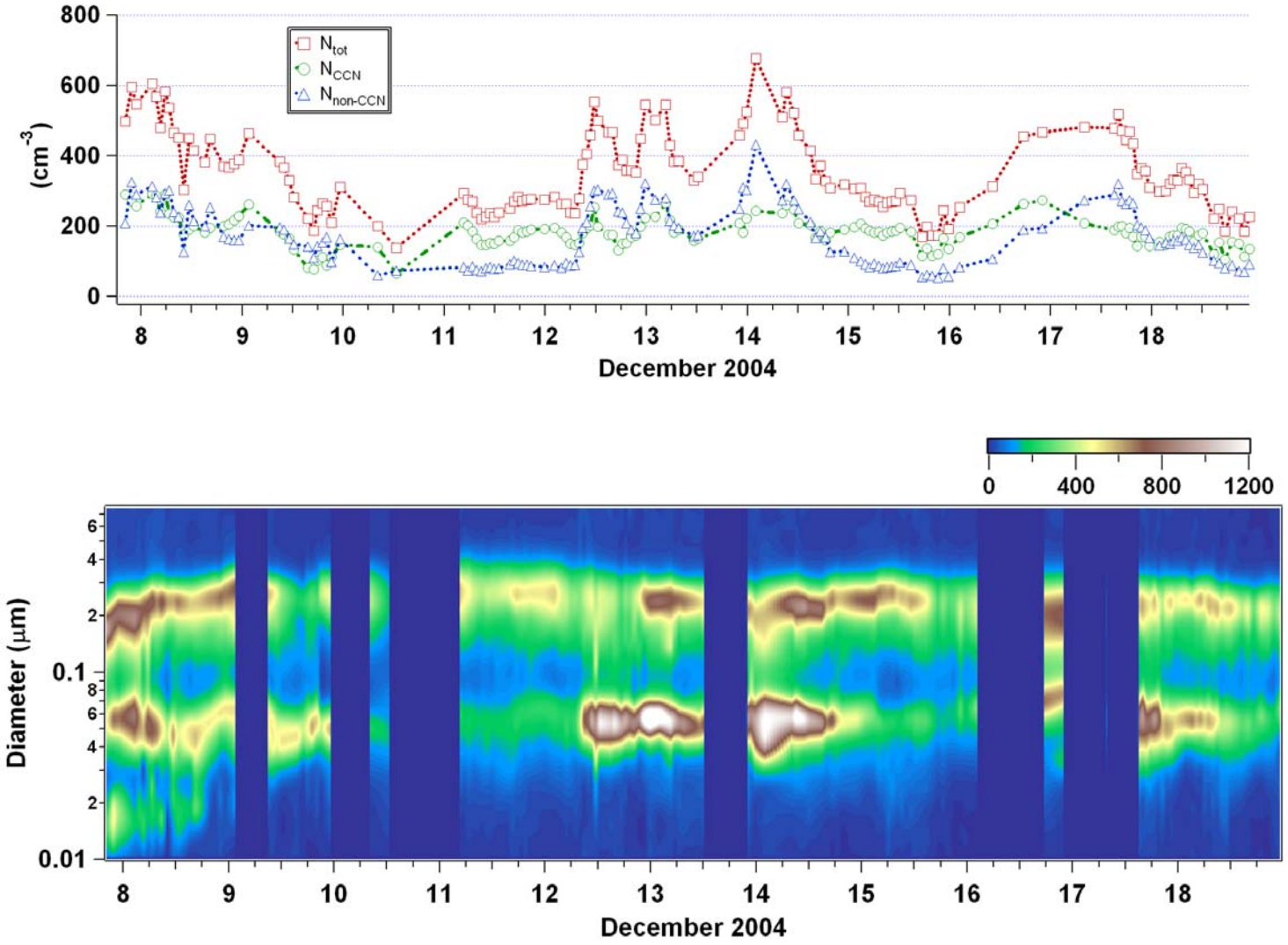

Figure 22. Upper panel :number concentration and lower panel aerosol number distribution as measured by the TDMA. The number distribution displays a strong bimodal distribution throughout the cruise. The number concentration is split into 3 categories; total concentration, CCN concentration, and non-CCN concentration.

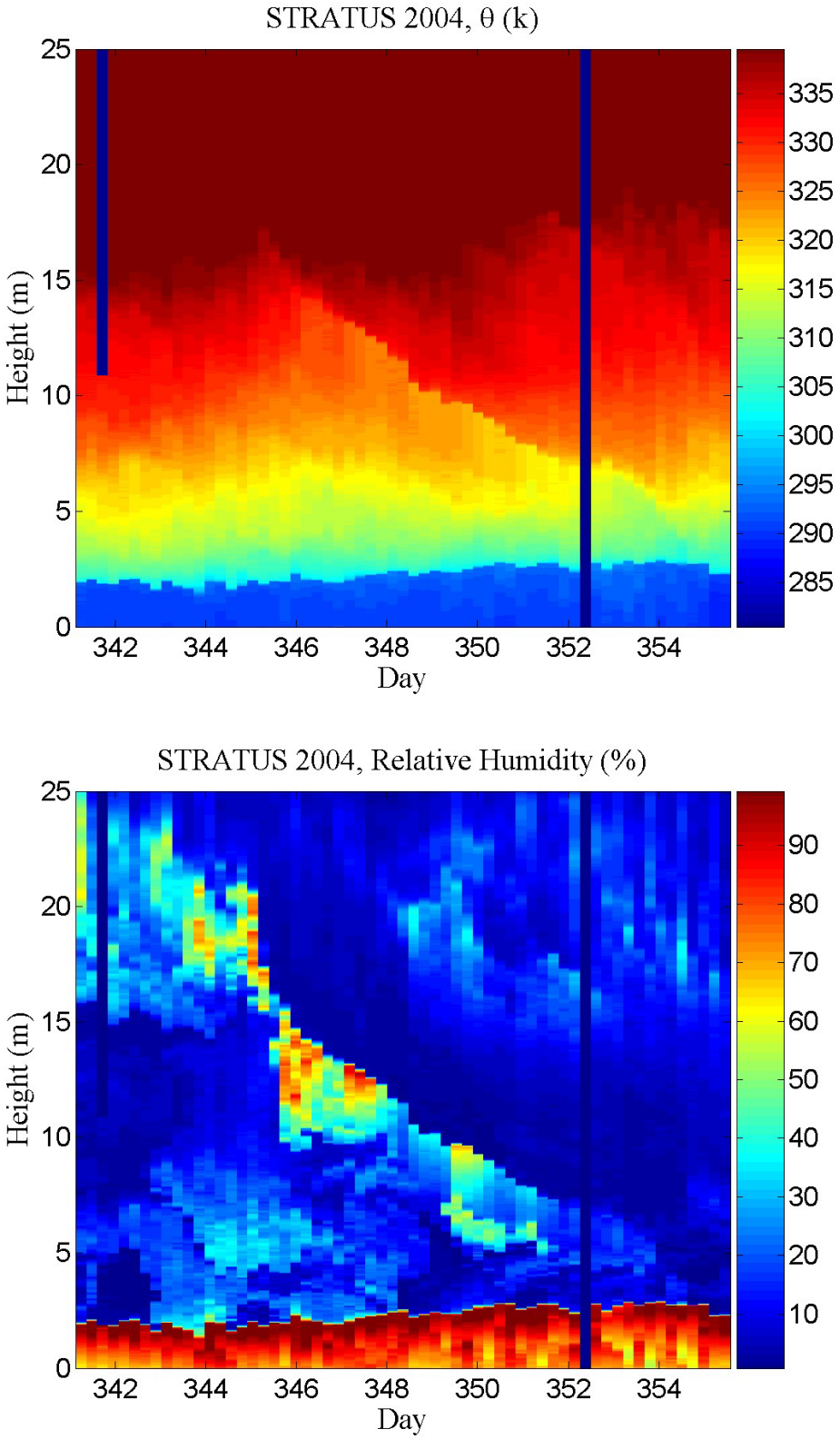

Figure 23. Time-height color contour plots from rawinsondes launched during the 2004 stratus cruise. The upper panel is potential temperature; the lower panel is relative humidity.

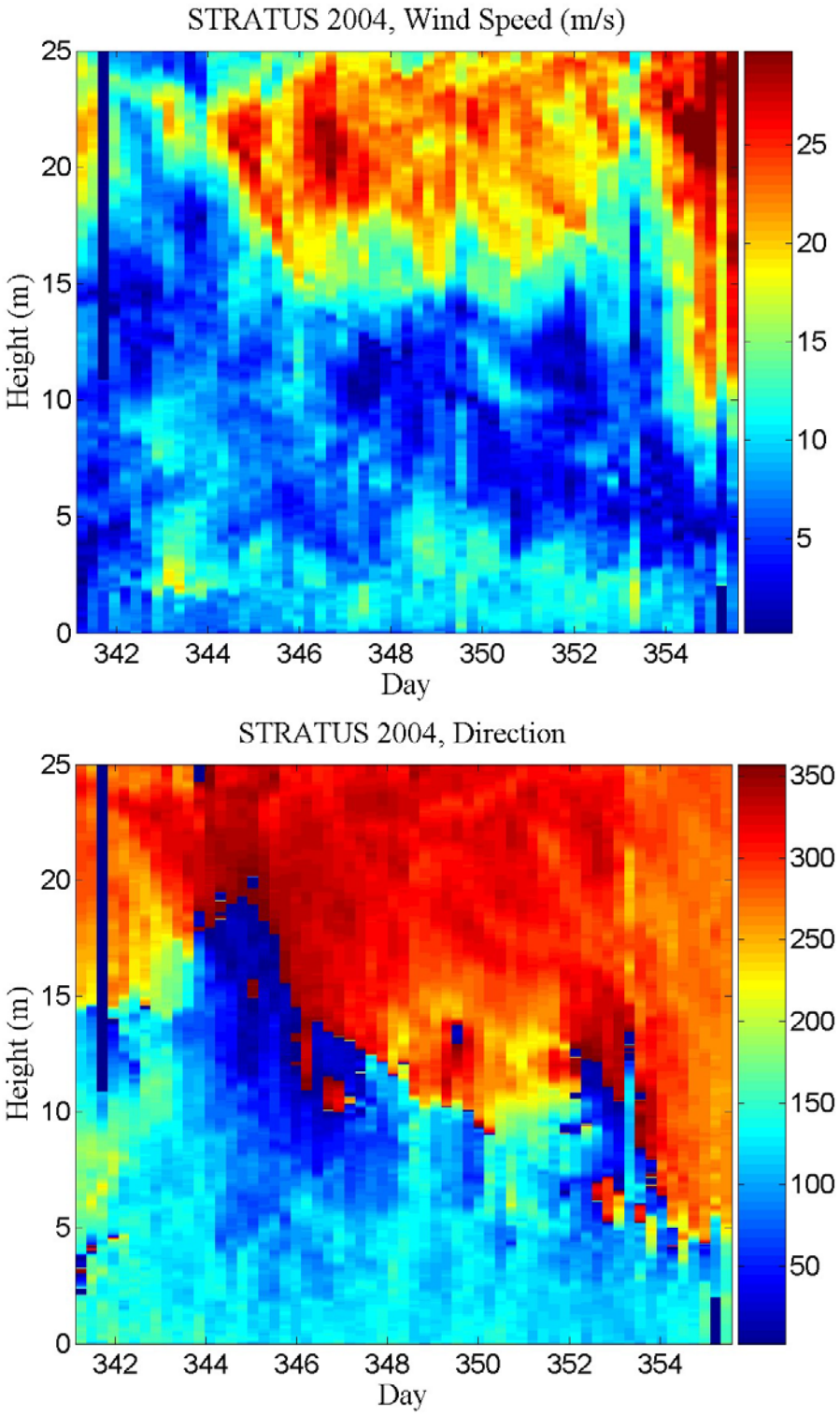

Figure 24. Time-height color contour plots from rawinsondes launched during the 2004 Stratus cruise. The upper panel is wind speed; the lower panel is wind direction.

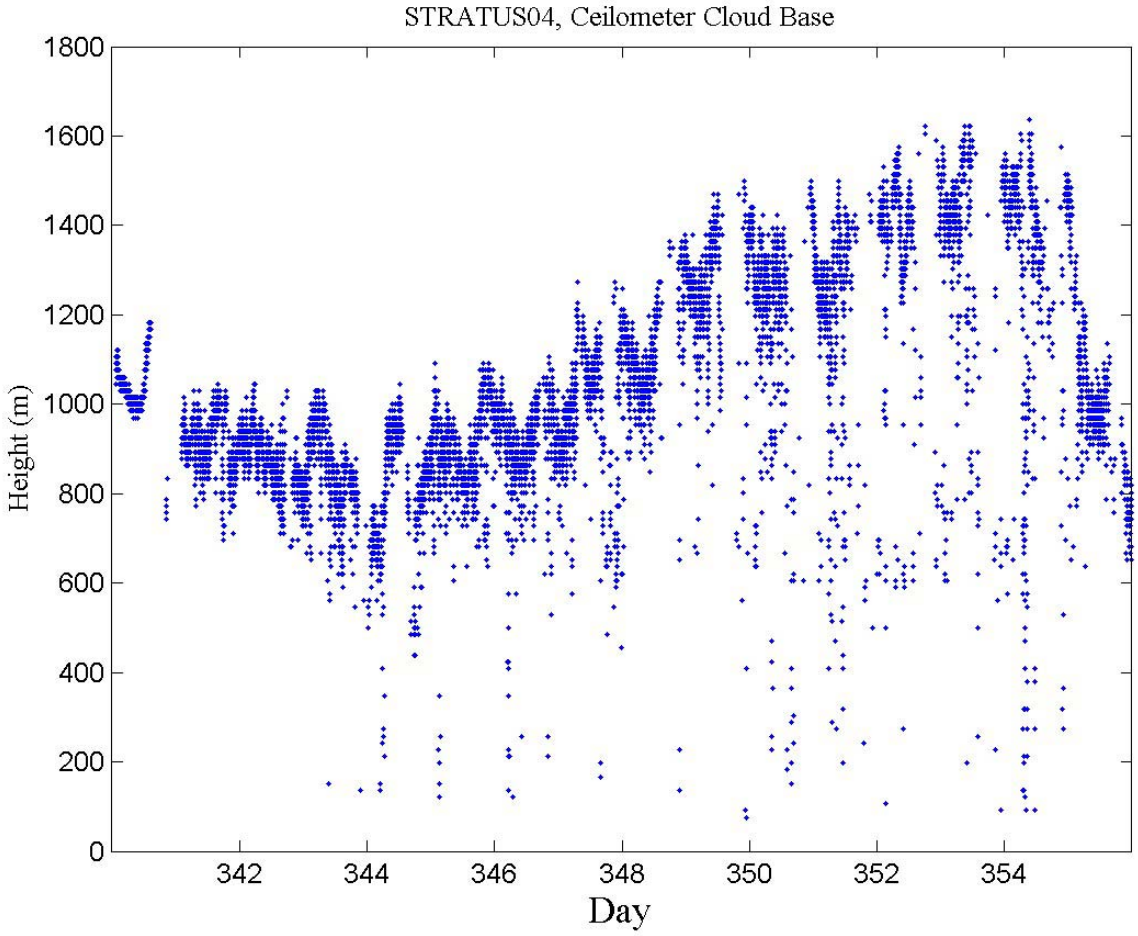

Figure 25. Time series of low cloud-base heights for the experimental period during December.

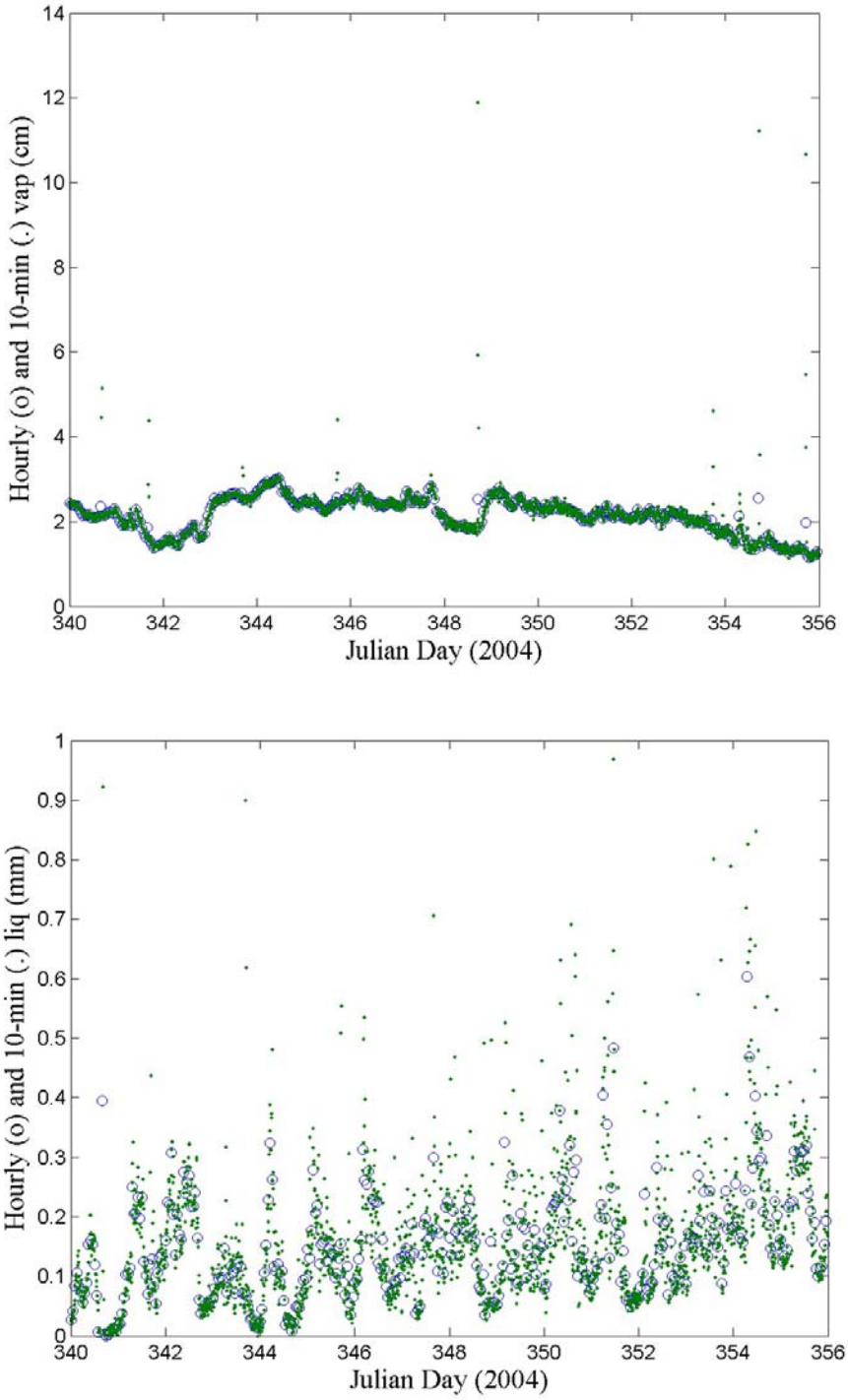

Figure 26. Time series of microwave radiometer-derived values for column integrated water vapor (upper panel) and column integrated liquid water (lower panel).

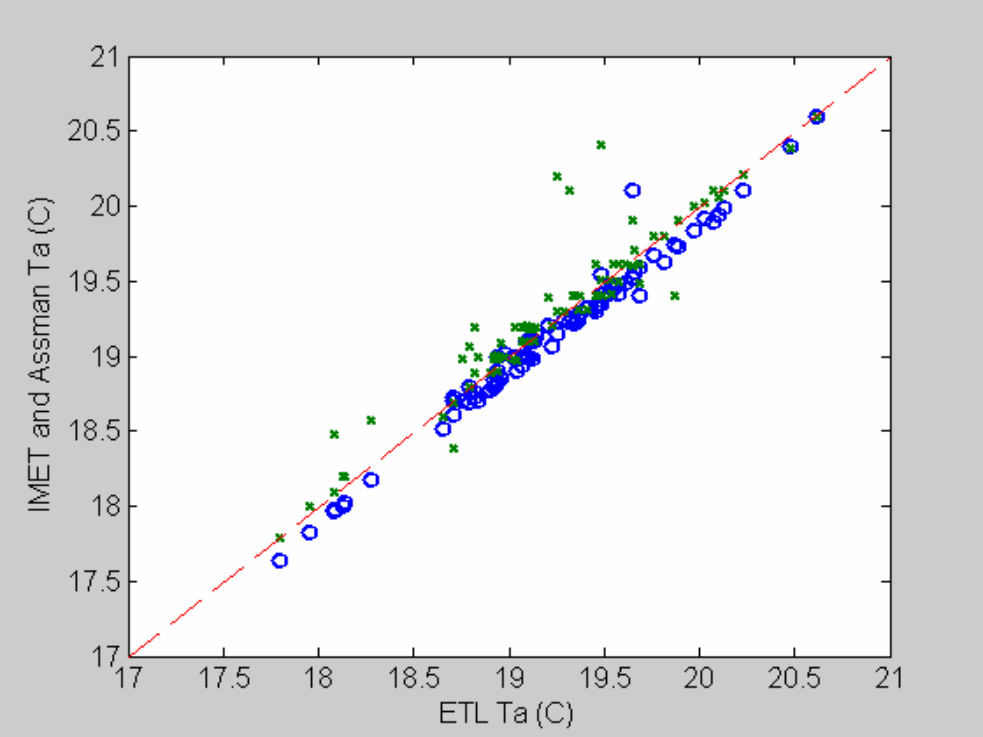

Figure 27. Comparison of simultaneous Assman psychrometer (x's) and ship (circles) readings for air temperature. Psychrometer values corrected to 15 m (ETL and ship instrument height).

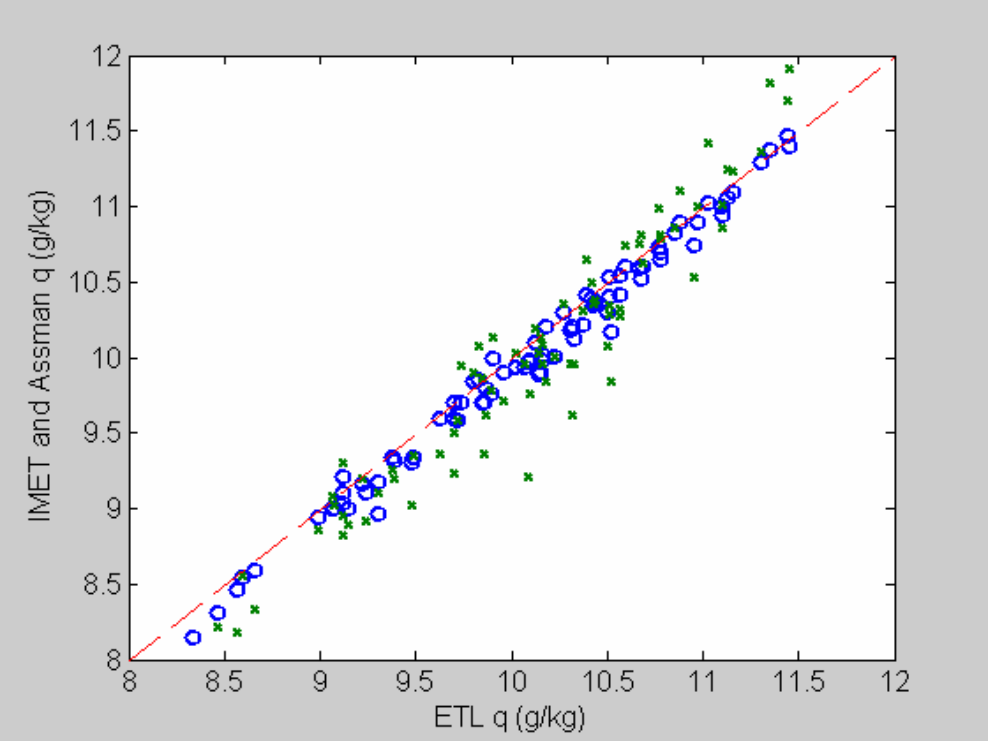

Figure 28. Comparison of simultaneous Assman psychrometer (x's) and ship (circles) readings for specific humidity. Psychrometer values corrected to 15 m (ETL and ship instrument height).

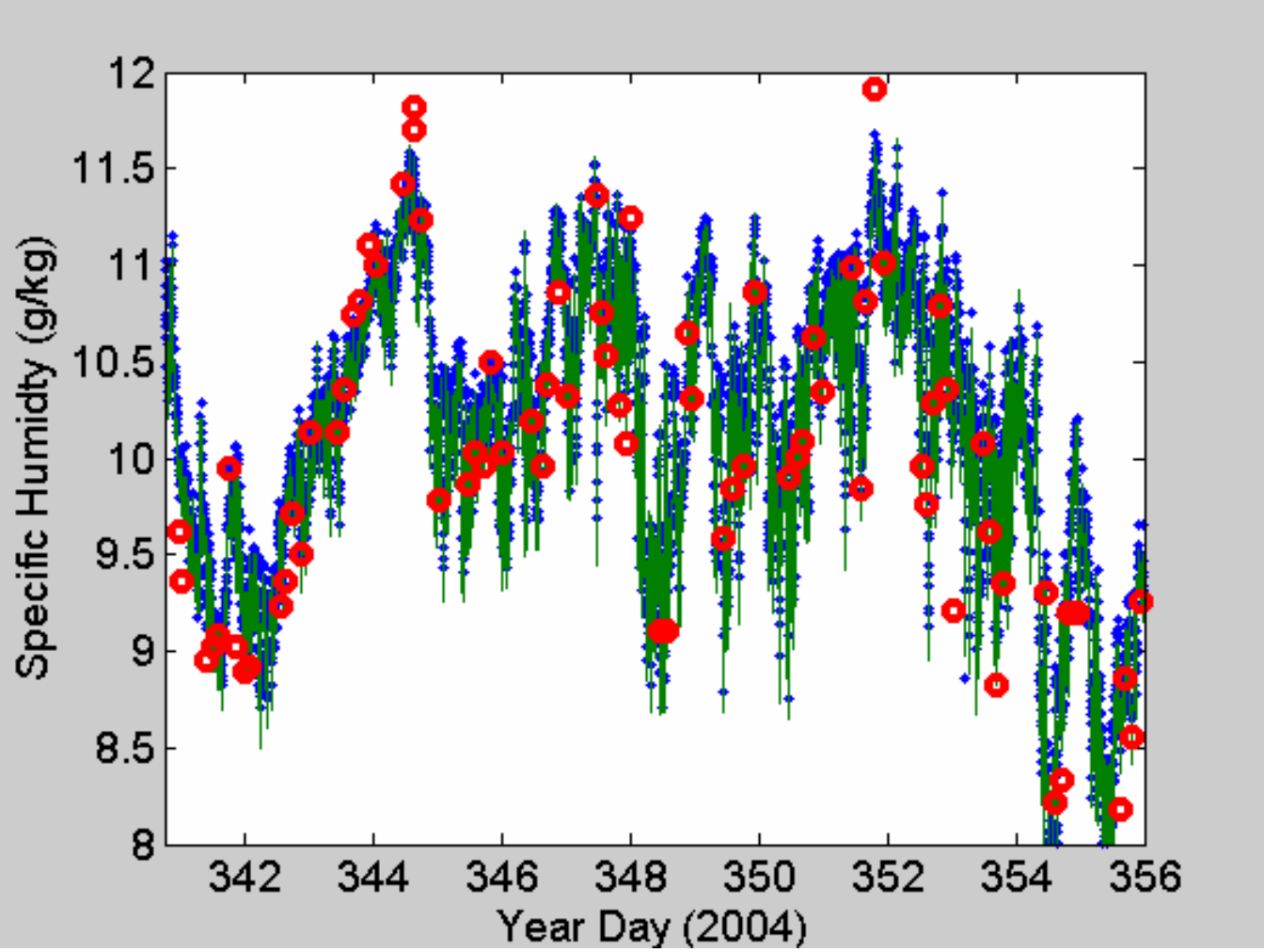

Figure 29. Time series of specific humidity for the Stratus04 cruise: ETL – blue, ship – green, red circles – psychrometer corrected to 15 m height.

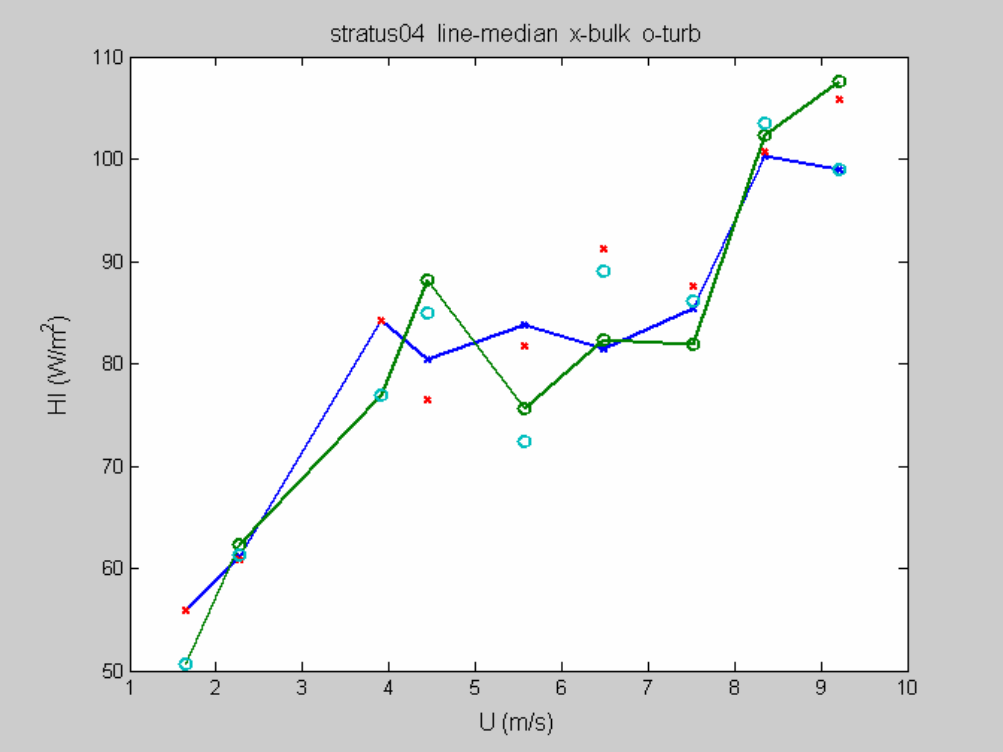

Figure 30. Latent heat flux averaged in wind-speed bins for the Stratus04 cruise: x-bulk values and o-direct values. Symbols with lines are medians; symbols without lines are means.

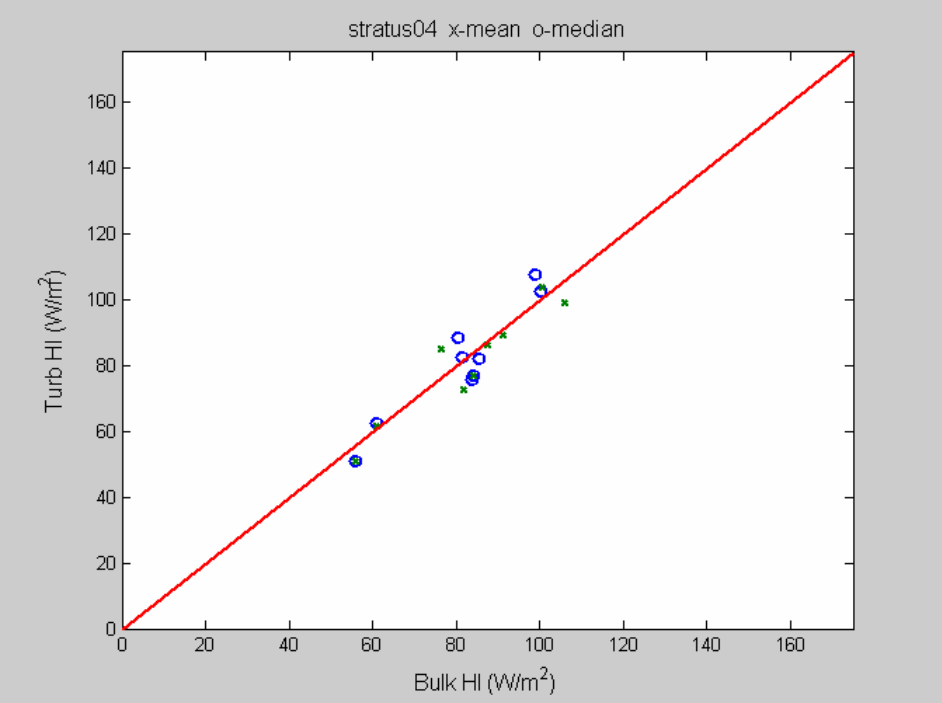

Figure 31. Average bulk latent heat flux vs direct values from wind speed bins (0 – 1 m/s) for the Stratus04 cruise: x-mean and o-median.